Syntectonic crustal melting and high-grade metamorphism in a transpressional regime, Variscan Massif Central, France

Aude Gébelin [a,b,c,*], Françoise Roger [a], Maurice Brunel [a]

[a] Université Montpellier II, Géosciences Montpellier, CNRS-UMR 5243, CC060, Place E.Bataillon, 34095 cedex5 Montpellier, France
[b] Department of Geology and Geophysics, University of Minnesota, Minneapolis, MN 55455, USA
[c] Institut für Geologie, Leibniz Universität Hannover, 30167 Hannover, Germany

ABSTRACT

Hot collisional orogens are characterized by abundant syn-kinematic granitic magmatism that profoundly affects their tectono-thermal evolutions. Voluminous granitic magmas, emplaced between 360 and 270 Ma, played a visibly important role in the evolution of the Variscan Orogen. In the Limousin region (western Massif Central, France), syntectonic granite plutons are spatially associated with major strike–slip shear zones that merge to the northwest with the South Armorican Shear Zone. This region allowed us to assess the role of magmatism in a hot transpressional orogen. Microstructural data and U/Pb zircon and monazite ages from a mylonitic leucogranite indicate synkinematic emplacement in a dextral transpressional shear zone at 313 ± 4 Ma. Leucogranites are coeval with cordierite-bearing migmatitic gneisses and vertical lenses of leucosome in strike–slip shear zones. We interpret U/Pb monazite ages of 315 ± 4 Ma for the gneisses and 316 ± 2 Ma for the leucosomes as the minimum age of high-grade metamorphism and migmatization respectively. These data suggest a spatial and temporal relationship between transpression, crustal melting, rapid exhumation and magma ascent, and cooling of high-grade metamorphic rocks.
Some granites emplaced in the strike–slip shear zone are bounded at their roof by low dip normal faults that strike N–S, perpendicular to the E–W trend of the belt. The abundant crustal magmatism provided a low-viscosity zone that enhanced Variscan orogenic collapse during continued transpression, inducing the development of normal faults in the transpression zone and thrust faults at the front of the collapsed orogen.

© 2009 Elsevier B.V. All rights reserved.

1. Introduction

The generation of abundant granitic magma, in part by crustal anatexis, is a characteristic feature of "hot" collisional orogens. However, the mechanisms of partial melting and the resulting consequences for the tectonic evolution of such orogens are still debated, partly due to the commonly deep levels of the crust at which these processes occur. Thus, the Variscan belt which exposes vast amounts of granitic intrusions, migmatitic complexes, and numerous scattered outcrops of granulite facies rocks offers a unique opportunity to study the role of partial melting during orogeny (Pin and Vielzeuf, 1983; Gapais et al., 1993; Brown and Dallmeyer, 1996; Vanderhaeghe et al., 1999; Ledru et al., 2001; Brown, 2004).

In the French Massif Central and southern Brittany, Variscan high-grade rocks located south of the Galicia–South Brittany suture (Fig. 1a) and associated with strike–slip shear zones (Fig. 1b) represent an excellent target to understand the thermomechanical processes associated with wrench zones that develop in a transpressional regime. Consequently, the role of partial melting and magma storage in the crust during orogeny can be evaluated by investigating the timing and structural relationships of magma generation and emplacement with first-order tectonic features such as major shear zones. Transpressional regimes give rise to complex geometries in orogenic belts and the finite strain patterns observed in such orogens cannot be related to plate kinematics in a straightforward fashion. This is particularly important in now deeply eroded orogens like the Variscan belt of central Europe.

Vanderhaeghe and Teyssier (2001) proposed that the presence of a layer of low-viscosity rocks in the middle crust could play a significant role in plate-scale deformation of thickened crust and changes in mid-crustal rheology have subsequently been correlated with rock uplift in orogenic belts (Liu and Shen, 1998; Meissner and Mooney, 1998; Godin et al., 2006; Hodges, 2006; Groome et al., 2008; Rey and Coltice, 2008). Moreover, the relative timing of changes in crustal buoyancy due to the combined effects of crustal thinning and partial melting may be a critical parameter in reconstructing the topographic evolution of eroded orogens (Mulch et al., 2007; Mulch and Chamberlain, 2007). Evaluating the thermal and structural history of "hot" orogenic crust deformed and/or exhumed in transpression is therefore a key aspect of understanding oblique tectonic regimes.

* Corresponding author. Tel.: +49 511 7623883; fax: +49 511 7622172.
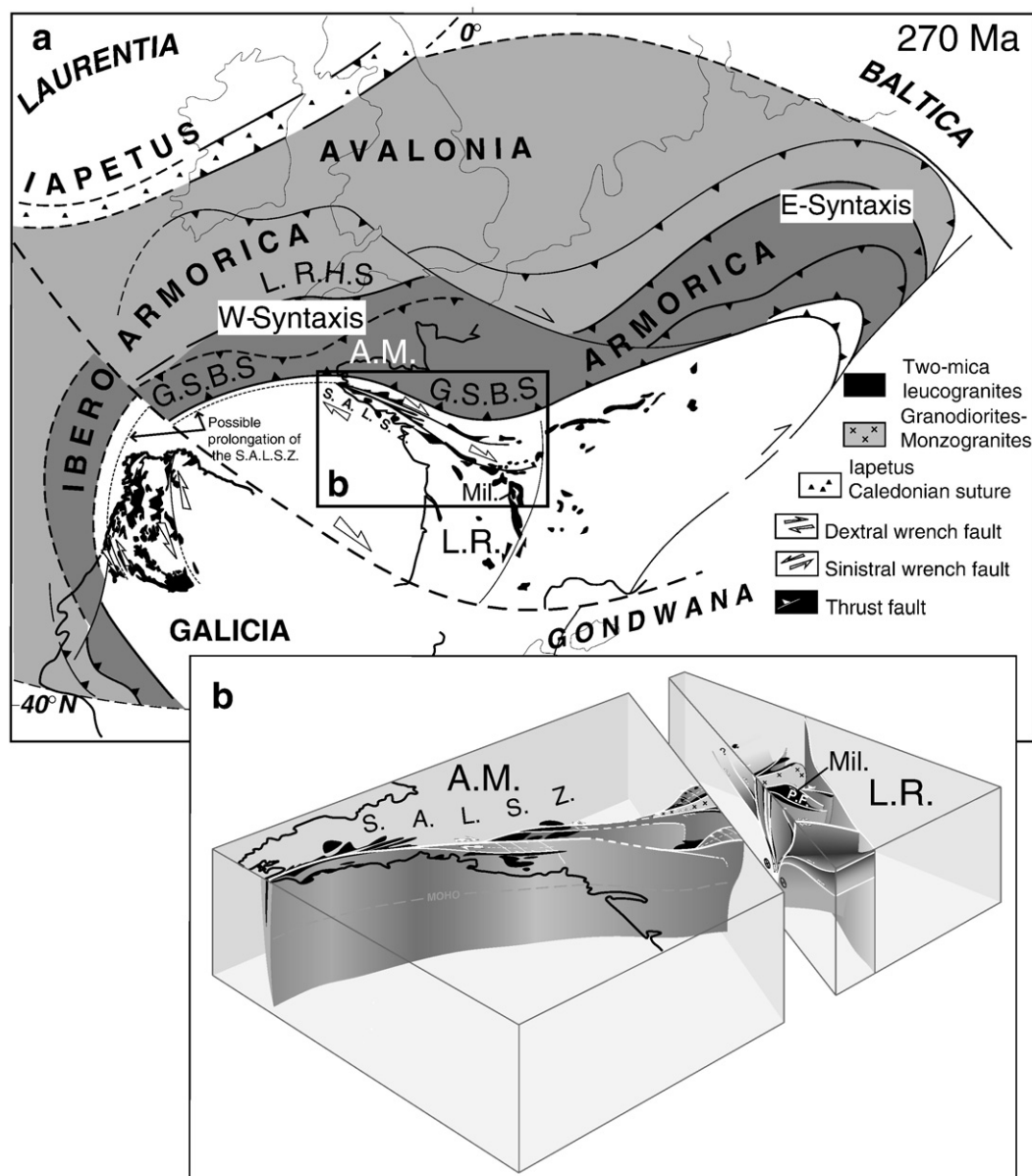E-mail address: gebelin@geowi.uni-hannover.de (A. Gébelin).

Fig. 1. (a) Current location of two-mica leucogranites within the Variscan Belt of western Europe at 270 Ma, according to Matte (2002). (b) 3-D geometry of pop-up structure affecting the Armorican Massif and the Limousin area at ca. 350 Ma, according to Gébelin et al. (2007). G.S.B.S., Galicia-South Brittany Suture; L.R.H.S., Lizard Rheno Hercynian Suture. S.A.L.S.Z., South Armorican Limousin Shear Zone; A.M., Armorican Massif; L.R., Limousin Region; and Mil., Millevaches.

Although the exhumation mechanisms for deep crustal rocks are rather well understood in extensional regimes (Teyssier and Whitney, 2002; Gilotti and Elvevold, 2002; Martiñez-Martiñez et al., 2004), the exhumation of orogenic crust in highly oblique regimes is not nearly as well documented. Even though high-grade metamorphic rocks exhumed along strike–slip zones have been studied using a variety of approaches (e.g. Leloup et al., 1995; Whitney et al., 2007), the relationships between metamorphism and crustal melting in transpressive tectonic regimes and the associated exhumation mechanisms remain debated. As an example, the Montagne Noire metamorphic core complex (SE France) has been interpreted either as a result of orogenic collapse due to gravitational instability after tectonic thickening (Van Den Driessche and Brun, 1991), by strike–slip faulting (Echtler and Malavieille, 1990), or to be a compressional post-nappe anticline with an anatectic core (Matte et al., 1998). Similarly, a Neoproterozoic metamorphic core complex in the Eastern Desert of Egypt is associated with strike–slip faults, but the exhumation of deep

crustal rocks in the complex is attributed to an increase of heat flow along the fault system generating syn-extensional plutonism that triggered the exhumation of the domes (Fritz et al., 1996). In the case of a dome/core complex system in a highly oblique (wrench) zone in central Anatolia, a migmatite dome formed during alternating transpression and transtension (Umhoefer et al., 2007). Wrenching of partially molten crust during crustal thinning and erosion drove exhumation (Whitney et al., 2003, 2007). These and other examples illustrate that high-grade metamorphism, crustal melting, deformation of orogenic crust, and exhumation are significant processes that may be associated with strike–slip faulting.

In this paper, we focus on the Limousin region (northwest part of the French Massif Central) and the Armorican massif (Fig. 1) where peraluminous leucogranite and high-grade metamorphic rocks are spatially associated with strike–slip shear zones. In particular, in the Millevaches massif (Limousin) the Pradines mylonitic fault, one of the biggest strike–slip zones of the Massif Central (Fig. 2a) is spatially and

temporally associated with partial melting and magmatism. This 4–5 km wide dextral strike–slip shear zone developed within two-mica leucogranite and high-grade metamorphic rocks. Previous work has documented the timing of syn-tectonic emplacement of the Millevaches granite in a transpressional regime (Gébelin et al., 2006, 2007) and provides a kinematic framework within which magmas were emplaced in a pop-up structure that spans the Armorican massif to the Limousin region and that was active from 350 to 300 Ma (Gébelin et al., 2007).

However, the timing of granite emplacement, deformation and associated high-grade metamorphic rocks and its bearing on the associated exhumation mechanisms in transpressional regimes are still not well understood. Here, we present a series of new U/Pb ages from two-mica leucogranite of the Pradines mylonites and associated high-grade metamorphic rocks. These geochronological data are the first obtained for this rock type in this part of the French Massif Central and are of great importance for the geodynamic model. Integrated with analysis of metamorphic pressure–temperature conditions, these results are compared with those acquired in the eastern part of the French Massif Central to better understand the possible origin of the thermal anomaly that induced large volume of crustal melts south of the Galicia–South Brittany suture. Discussed in the geodynamic context of the Variscan belt, this new data set allow us to best precise the conditions and timing of metamorphism, crustal melting, and deformation, and to get subsequent evaluation of the relationship of these processes to the oblique tectonic regime during crustal thickening and exhumation.

2. Geological framework

2.1. Major tectono-metamorphic events

The West European Variscan Belt is a collisional belt that experienced crustal thickening (350–310 Ma; Matte, 1986, 1991) followed by extension and thinning (335–290 Ma; Van den Driessche and Brun, 1989; Faure et al., 1990; Burg et al., 1990; Faure, 1995; Faure et al., 2002). In the French Massif Central, Variscan events range from high-pressure (HP) metamorphism in the Late Silurian–Early Devonian (440–400 Ma) to deposition of late orogenic sediment in the Late Carboniferous–Early Permian (300 Ma) (Pin and Vielzeuf, 1983; Ledru et al., 1989; Santallier et al., 1994; Faure et al., 1997; Matte et al., 1998).

Two gneissic units are distinguished throughout most of the Massif Central (Burg et al., 1984; Santallier et al., 1988; Ledru et al., 1989, 1994; Ledru et al., 1994; Lardeaux et al., 2001) (Fig. 2a): The upper gneiss unit (UGU) contains HP metamorphic assemblages (up to 28 kbar; Lardeaux et al., 2001). The UGU overlies a lower gneiss unit (LGU) that lacks the HP metamorphic assemblages and is characterized by abundant migmatites. The presence of syn-kinematic cordierite in the migmatitic metasedimentary gneiss of the LGU may be related to high-temperature (HT) decompression of the HP metamorphic assemblages (Mercier et al., 1992; Santallier et al., 1994) under medium-P and high-T conditions (5–6 kbar, 760–780 °C (Le Breton and Thompson, 1988)). This high-T metamorphism is dated in the Limousin area at 354.0 ± 4.8 Ma (U–Th/Pb monazite; Gébelin, 2004).

Late Carboniferous post-orogenic extension (Ménard and Molnar, 1988; Van Den Driessche and Brun, 1991; Faure, 1995) was marked by the development of conjugate dextral and sinistral ductile wrench faults contemporaneous with magma emplacement (Arthaud and Matte, 1977; Guineberteau et al., 1987; Gébelin et al., 2007). These late-orogenic events are contemporaneous with a major thermal anomaly characterized by emplacement of basic magmas and associated high-grade metamorphism at 300 ± 20 Ma in granulites of the eastern part of the French Massif Central (Pin and Vielzeuf, 1983). Late anatectic thermal domes such as the Velay dome (Fig. 2a)

emplaced during the same period (Ait Malek, 1997; Mougeot et al., 1997; Be Mezeme, 2005) can be related to the same event (Ledru et al., 2001).
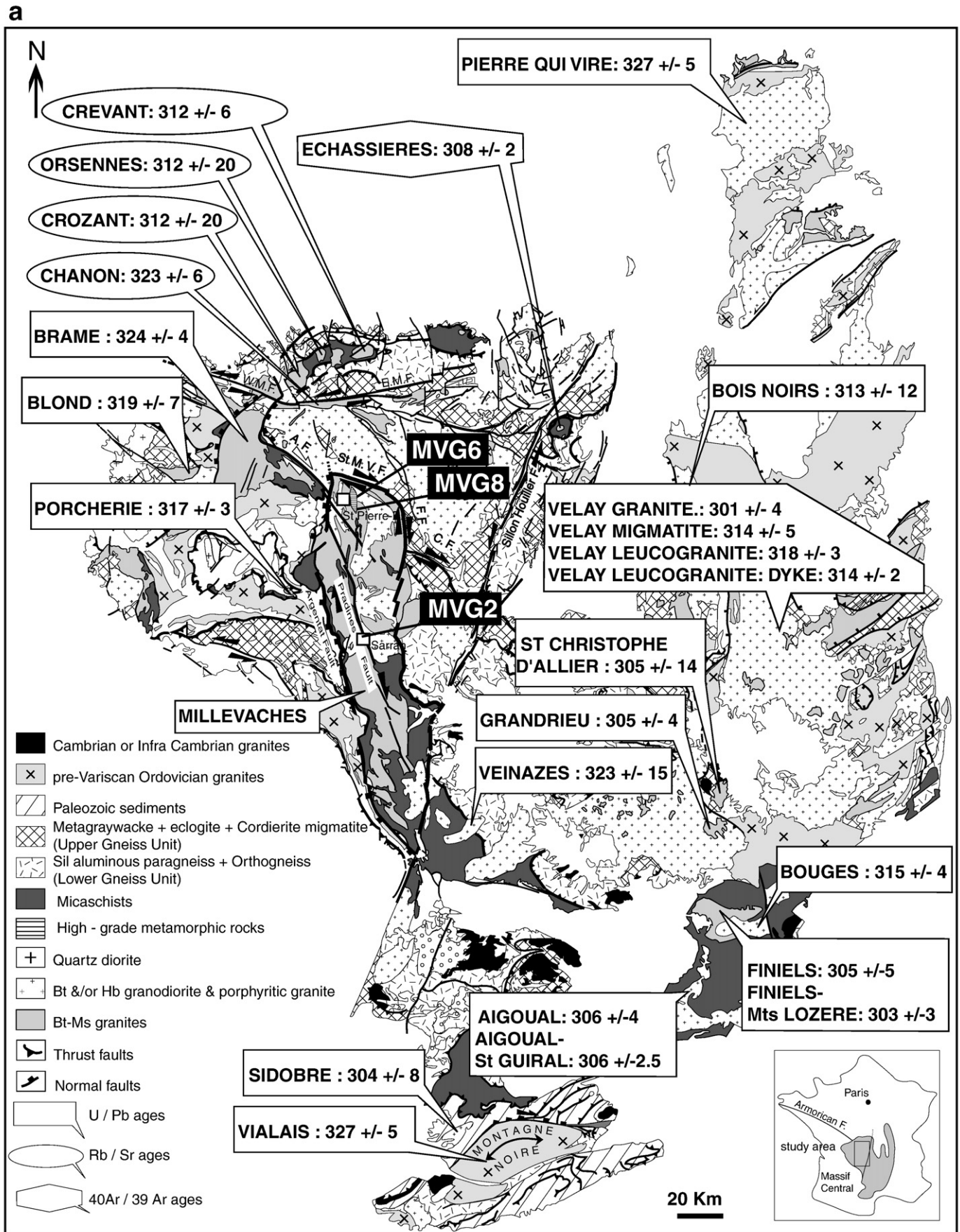
2.2. Limousin geological setting

In the Limousin area, two main types of granites are spatially associated with N–S trending normal shear zones and large E–W to NW–SE strike–slip ductile shear zones (Fig. 2a): (1) peraluminous granodiorite emplaced between 356 ± 5 Ma and 349 ± 5 Ma (U–Pb zircon, Bertrand et al., 2001); their emplacement marked the end of nappe tectonics; and (2) two-mica leucogranite generated by partial melting of metasedimentary middle to lower crust and emplaced during the late stages of Variscan orogeny (330–310 Ma) (Cuney et al., 1990, Downes et al., 1990, Williamson et al., 1996). The two-mica leucogranite is spatially and temporally associated with high-grade metamorphic rocks. Previous investigations have emphasized the role of late-orogenic extension in the emplacement of these two-mica leucogranites (Faure, 1989; Faure and Pons, 1991; Faure, 1995). In contrast, new structural, geophysical and geochronological data support ascent and emplacement along a dextral shear zone active from 350 to 300 Ma in a transpressional regime (Gébelin et al., 2006, 2007).

Two-mica leucogranites occur as horizontal laccoliths with an estimated thickness of ≤4 km (Gébelin et al., 2004, 2006). One example, the 160 km long, N–S trending Millevaches massif (Fig. 2a) consists of biotite ± cordierite-bearing porphyritic granite and two-mica leucogranite hosted by micaschists. The N–S dextral strike–slip Pradines shear zone affected granite and high-grade metamorphic rocks over a 5-km-wide zone (Fig. 2a).

The deformation of biotite ± cordierite-bearing porphyritic granite at a magmatic stage (Fig. 3a) and biotite–muscovite C–S structures (Fig. 3b–c) observed in the two-mica leucogranite, suggest that the Pradines shear zone was active during magma emplacement. Right-lateral wrenching is expressed at the map scale in the sigmoidal pattern of magnetic foliations and lineations within the granite, (Gébelin et al., 2006). Magnetic lineations gradually rotate from NNW–SSE in the centre of the shear zone to NW–SE outside. Magnetic foliations are generally steep in the centre and become gradually flatter until they attain a sub-horizontal orientation outside the shear zone. The proposed model of emplacement includes magma ascent along the vertical strike–slip Pradines fault, which channelled magmas from depth to their middle crustal emplacement level followed by lateral migration along the pre-existing horizontal foliation (Gébelin et al., 2004, 2006). The Millevaches massif is fault bounded to the west, by the brittle–ductile Argentat normal fault (Figs. 2a–9;Lameyre, 1984; Ledru and Autran, 1987; Mattauer et al., 1988) and to the north and east by dextral strike–slip faults.

3. Petrography and mineral compositions

Representative samples of mylonitic two-mica leucogranite (MVG2) and high-grade, migmatitic metasedimentary gneiss (MVG6 and MVG8) were selected for detailed analysis of structures, metamorphic conditions and ages. Samples were examined in outcrop and thin sections. Major element compositions of minerals were determined by EMPA on a CAMECA SX-100 instrument equipped with five wavelength-dispersive X-ray spectrometers (WDS) at Service Microsonde Sud (Université Montpellier 2). Analyses were undertaken using an accelerating voltage of 20 kV and beam current of 10 nA. Concentrations are obtained from raw intensities using the "X-PHI" quantification procedure (Merlet, 1994). Natural minerals, synthetic oxides and pure metals are used as standards. Representative mineral compositions for garnet, biotite, cordierite, K-feldspar and plagioclase are given in Table 1 for MVG6 and MVG8.

a

N

PIERRE QUI VIRE: 327 +/- 5

CREVANT: 312 +/- 6

ORSENNES: 312 +/- 20

ECHASSIERES: 308 +/- 2

CROZANT: 312 +/- 20

CHANON: 323 +/- 6

BRAME : 324 +/- 4

BOIS NOIRS : 313 +/- 12

BLOND : 319 +/- 7

MVG6
MVG8

PORCHERIE : 317 +/- 3

VELAY GRANITE.: 301 +/- 4
VELAY MIGMATITE: 314 +/- 5
VELAY LEUCOGRANITE: 318 +/- 3
VELAY LEUCOGRANITE: DYKE: 314 +/- 2

MVG2

ST CHRISTOPHE
D'ALLIER : 305 +/- 14

MILLEVACHES

GRANDRIEU : 305 +/- 4

VEINAZES : 323 +/- 15

BOUGES : 315 +/- 4

FINIELS: 305 +/-5
FINIELS-
Mts LOZERE: 303 +/-3

AIGOUAL: 306 +/-4
AIGOUAL-
St GUIRAL: 306 +/-2.5

SIDOBRE : 304 +/- 8

VIALAIS : 327 +/- 5

20 Km

Legend:
- Cambrian or Infra Cambrian granites
- pre-Variscan Ordovician granites
- Paleozoic sediments
- Metagraywacke + eclogite + Cordierite migmatite (Upper Gneiss Unit)
- Sil aluminous paragneiss + Orthogneiss (Lower Gneiss Unit)
- Micaschists
- High - grade metamorphic rocks
- Quartz diorite
- Bt &/or Hb granodiorite & porphyritic granite
- Bt-Ms granites
- Thrust faults
- Normal faults
- U / Pb ages
- Rb / Sr ages
- 40Ar / 39 Ar ages

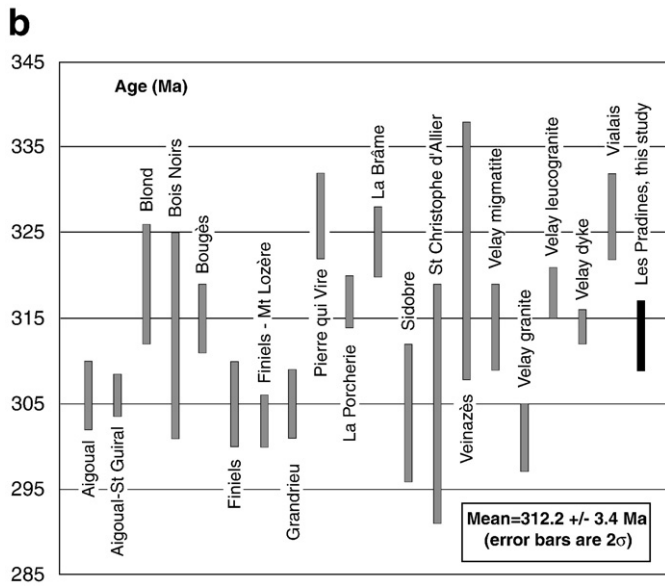Inset map: Paris, Armorican F., study area, Massif Central

b

Fig. 2. a: Geological map of the Massif Central showing 1) the sample locations for U–Pb geochronology in the Millevaches massif, 2) the location and ages (Ma) of leucogranites displaying similarities in age, deformational and field relationships with the Millevaches granites in the Limousin region, and 3) the location and ages (Ma) of granite emplacement in the East part of the French Massif Central consistent with those of the Limousin region. Our statement about similarity of leucogranites of the Limousin region with the Millevaches granites is based on the following data: Brâme two-mica syntectonic granite (Mollier and Bouchez, 1982; Holliger et al., 1986; Audrain et al., 1989; Faure et al., 1990; Faure and Pons, 1991; Scaillet et al., 1996; Le Carlier de Veslud et al., 2000); Blond syntectonic leucogranite (Scaillet et al., 1996; Alexandrov et al., 2000; Le Carlier de Veslud et al., 2000); Porcherie two-mica granite (Lafon and Respaut, 1988); Crevant two-mica syntectonic granite (Petitpierre and Duthou, 1980; Gébelin et al., 2006); syntectonic Crozant and Orsennes two-mica granites (Rolin et al., 1982; Dumas et al., 1990; Gébelin et al., 2006); Chanon syntectonic leucogranite (Choukroune et al., 1983; Quenardel et al., 1991). Compilation of granite emplacement ages for Massif Central from: Aigoual granite, Bougès granite, Finiels granite and Veinazes granite (Monié et al., 2000); Aigoual — Saint Guiral and Finiels-Mt Lozère (Brichau et al., 2008); Bois noirs granite (Binon and Pin, 1989); Grandrieu granite (Lafon and Respaut, 1988); Pierre qui vire (Supply, 1985); Sidobre granite (Pin, 1991); Vialais granite (Matte et al., 1998); Velay granite and Velay migmatite (Mougeot et al., 1997); Velay leucogranite and Velay leucogranite dyke (Be Mezenne, 2005); Echassières leucogranite (Cheilletz et al., 1992); St Christophe d'Allier (Isnard, 1996). b: U/Pb ages for granites of the French Massif Central (see Fig. 2a).

The bulk composition (major and some minor elements) for MVG6 and MVG8 was determined by XRF from CRPG (Centre de Recherches Pétrographiques et Géochimiques, France) of Nancy (Table 2).

3.1. Mylonite of two-mica leucogranite

Mylonitic leucogranite such as MVG2 characterizes the NNW–SSE Pradines dextral strike–slip shear zone (Fig. 2a). Sample MVG2 is composed of K-feldspar (orthoclase or microcline), plagioclase (albite or oligoclase, An_4–An_{12}), quartz, biotite, and muscovite. The mylonite displays a NNW–SSE striking foliation that dips steeply to the east (>55°) and contains a near horizontal stretching lineation. Biotite–muscovite C–S structures indicate a dextral sense of shear (Fig. 3b–c) and quartz grain boundaries form a mosaic pattern (Fig. 3d).

3.2. High-grade metamorphic rocks

High-grade metamorphic rocks occur as NNW–SSE oriented vertical lenses in the Pradines fault zone (Fig. 2a). Their internal foliation strikes N–S to NNW–SSE with a vertical dip. Two main rock types characterize these lenses: biotite–garnet–sillimanite–cordierite gneiss (Fig. 3e) and garnet–cordierite gneiss (Fig. 3f). Field observations show an increase in inferred granitic melt fraction from the biotite–garnet–sillimanite–cordierite gneiss into the garnet–cordierite gneiss which leads us to describe these two-types of rocks as migmatite paleosome/mesosome (MVG6) and migmatite leucosome (MVG8), respectively.

Sample MVG6 is composed of K-feldspar, plagioclase, quartz, biotite, garnet, sillimanite, and cordierite ± ilmenite ± spinel. This rock shows, at the macroscopic scale, a subhorizontal layering formed alternately by i) 2–4 cm elongated single crystals of garnet, ii) the assemblage biotite + sillimanite + cordierite, and iii) single crystals of mm-thick ribbon cordierite, up to 4 cm in length (Fig. 3e). Deformed single crystals of garnet (Fig. 3e), microfolds of quartz, and garnet ribbons (Fig. 4a) are consistent with a dextral sense of shear.

Garnet crystals in this sample are commonly pancake-shaped with a XY:XZ:YZ ratio of 1:0.1:0.1 ratio (Fig. 4b) and are in metamorphic equilibrium with biotite, cordierite and sillimanite (Figs. 4b and 5a). Typical garnet compositions are $Alm_{76}Sps_1Prp_{14}Grs_2$ in the core with an increase in the Fe/Mg ratio towards the rim (Fig. 5a–b). Garnets typically contain inclusions of ilmenite, biotite and prismatic sillimanite. Sillimanite inclusions are very abundant in garnet cores (Fig. 4b). Some garnets are rimmed by cordierite (Fig. 4c), and are associated with sillimanite and biotite (Fig. 4d). These textural features can be attributed to high-T decompression (Brown and Dallmeyer, 1996; Johnson and Brown, 2004; White et al., 2004). Cordierite–sillimanite–biotite forms also pressure shadows whose asymmetry is consistent with a dextral sense of shear (Fig. 4e). Biotite is euhedral and Ti-rich ($3 < TiO_2 < 5.5$). Muscovite is absent. The plagioclase is of an oligoclase-type and displays no chemical zonation.

The representative leucosome (MVG8) has a fine- to medium-grained (1–3 mm) texture with a weakly defined foliation. In places, it shows shear bands indicating dextral strike–slip movement of the Pradines shear zone. The sample is characterized by up to 40% of cordierite (Fig. 4f), K-feldspar, plagioclase (oligoclase), quartz, garnet and rare biotite and sillimanite.

Cordierite and garnet are homogeneously distributed through the rock (Fig. 3f). Cordierite ($X_{Mg} = 0.59$) forms large, euhedral crystals (Fig. 4f), some of which are inclusion rich and contain rounded inclusions of ilmenite and hercynitic spinel. Garnet is light pink in colour and Fe-rich composition ($Alm_{73}Sps_3Prp_{17}Grs_2$) (Table 1). Biotite has very similar pleochroism and composition to the biotite observed in the paleosome.

4. Metamorphic conditions

The coexistence of sillimanite and K-feldspar and the absence of muscovite in quartz-bearing high-grade metamorphic rocks suggests the metamorphic reaction:

muscovite + quartz = K-feldspar + sillimanite + H_2O ± melt.

Gneiss in this region typically contains leucocratic veins and layers (i.e. leucosomes) that indicate partial melting. Because different parts of the gneiss have lost or gained components during migmatization, it is difficult to determine a representative bulk composition to calculate realistic pseudosections. Therefore pressure–temperature conditions were evaluated for metasedimentary gneiss MVG6 and migmatite leucosome MVG8 (See location Fig. 2a) using the THERMOCALC average P–T method in the NCKFMASH system (Holland and Powell, 1998; with updates) (Table 3). Average pressures and temperatures with their uncertainties (±1 sigma) are derived from the independent set of equilibria for each sample. As shown in Fig. 5b, compositional profiles show that garnets from MVG6 are chemically homogeneous except for a thin rim which displays an increase of XFe with respect to the garnet core. From the inner to the outer part this zoned rim displays a decrease in pyrope content, an increase in almandine content and a moderate increase in spessartite content (Fig. 5b). We interpret the Fe and Mg zoning in garnet as the result of
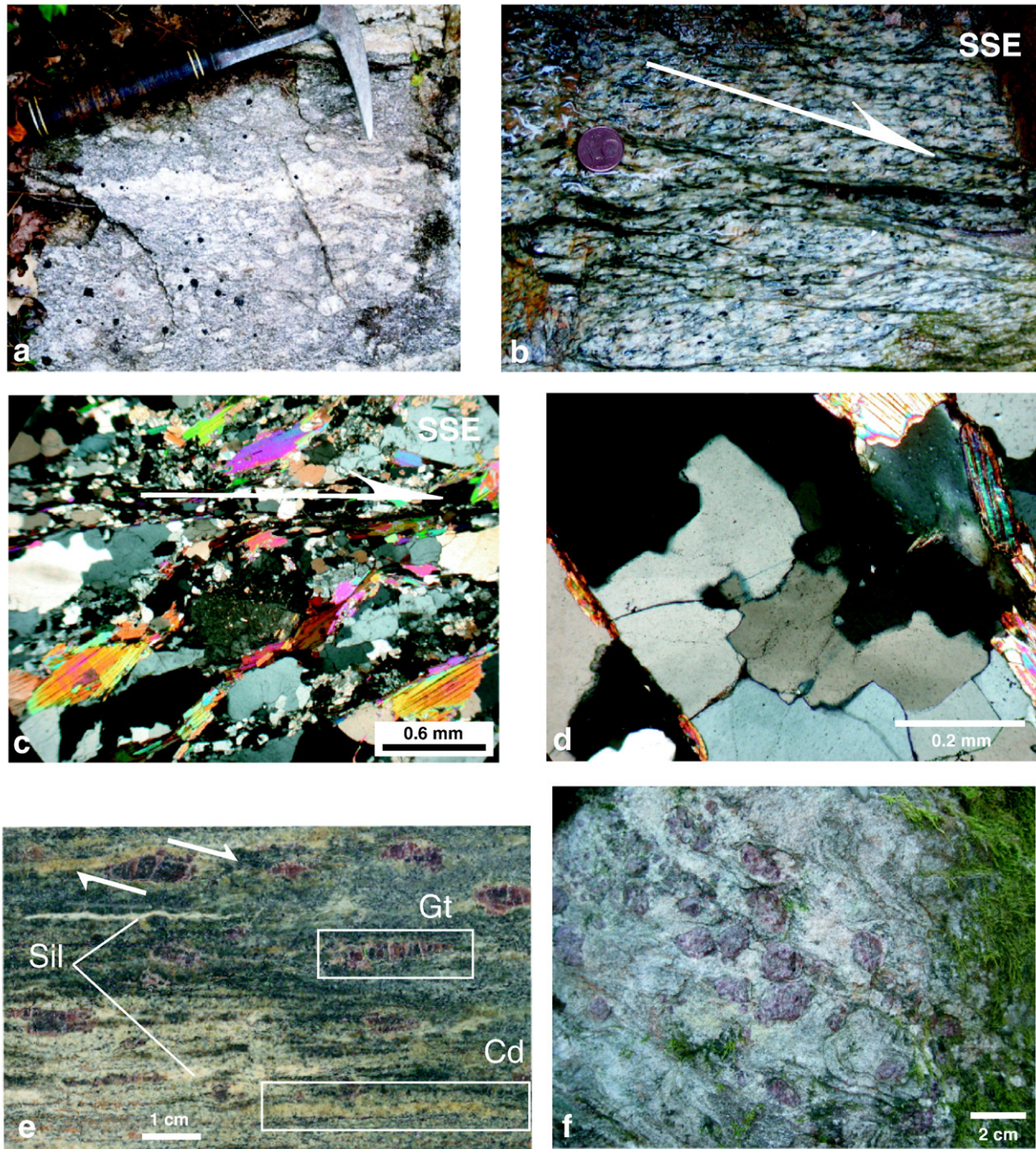
Fig. 3. (a) Porphyritic biotite granite deformed during under magmatic conditions. (b) Two-mica leucogranites of the Pradines fault zone, showing typical C–S structures indicating a dextral sense of shear. (c) Two-mica leucogranite of the Pradines fault zone, showing C–S structures defined by magmatic muscovite and biotite. (d) Quartz microstructures within foliated two-mica leucogranite of the Pradines fault zone, showing a blocky mosaic pattern typical of high temperature deformation. (e) Mesosome of high-grade metamorphic rocks in the XZ plane showing cm-sized flattened ribbon garnets, surrounded by 5 mm thick cordierite ribbons, quartz ribbons and biotite–sillimanite layers. (f) Leucosome of high-grade metamorphic rocks showing cordierite and centimeter–scale garnets sparsely distributed through the rock.

post-peak equilibration between cordierite and garnet during high-T decompression (Brown and Dallmeyer, 1996; Johnson and Brown, 2004; White et al., 2004). This interpretation is consistent with cordierite reaction rims around garnet (Fig. 4c). To avoid a potential bias to post-crystallization conditions, the average $P–T$ method has only been applied using garnet core compositions (Table 1). The results of the average $P–T$ method for the gneiss suggest equilibration of the gneiss at 6.1 ± 0.8 kbar and $836° \pm 57$ °C (using a H_2O activity-composition of 1) and at 5.7 ± 0.8 kbar and $810° \pm 54$ °C (best sigfit using a H_2O and CO_2 activity–composition of 0.8 and 0.2, respectively)

(Table 3). Pressures and temperatures calculated for MVG6 with the average PT mode of Thermocalc are consistent with those deduced from generic $P–T$ diagrams (White et al., 2004; White et al., 2007).

The "average $P–T$" method has been applied on garnet from sample MVG8 that, as seen in X-ray element maps (Fig. 5c), does not show any significant zoning other than a very slight enrichment of Mn in the core. Calculations using the average $P–T$ mode (garnet cores) yields 6.1 ± 1.1 kbar, 805 ± 62 °C (best obtained sigfit using a H_2O and CO_2 activity–composition of 0.9 and 0.1, respectively) and 5 ± 1.1 kbar, 758 ± 53 °C (using a H_2O and CO_2 activity–composition of 0.5 and 0.5)

Table 1
Representative mineral compositions from high-grade metamorphic rocks.

	MVG6	MVG6	MVG6	MVG6	MVG6	MVG8	MVG8	MVG8	MVG8	MVG8
	Crd	Grt-c	Bt	Pl	Kfs	Crd	Grt-c	Bt	Pl	Kfs
SiO_2	47.79	36.90	35.28	63.50	64.41	48.63	36.53	34.95	62.28	64.21
TiO_2	<d.l.	0.02	4.86	n.a.	–	0.02	0.02	3.18	n.a.	n.a.
Al_2O_3	32.78	21.55	17.44	23.21	19.40	33.23	21.42	18.68	23.71	19.08
FeO	9.92	36.09	20.50	n.a.	–	9.47	35.82	17.68	n.a.	n.a.
MnO	0.07	0.62	0.04	n.a.	–	0.13	1.64	0.02	n.a.	n.a.
MgO	7.34	4.79	8.45	n.a.	–	7.70	4.5	10.48	n.a.	n.a.
Cr_2O_3	<d.l.	<d.l.	0.07	n.a.	–	<d.l.	<d.l.	0	n.a.	n.a.
CaO	<d.l.	0.64	0.01	3.90	0.10	0.01	0.71	<d.l.	4.61	0.08
Na_2O	0.16	<d.l.	0.14	9.52	2.13	0.22	<d.l.	0.23	8.80	1.77
K_2O	<d.l.	<d.l.	10.28	0.36	13.19	<d.l.	<d.l.	9.34	0.60	15.01
Total	98.06	100.62	97.08	100.49	99.22	99.40	100.65	94.57	100.00	100.14
Cations										
Si	4.97	2.93	2.67	2.80	2.97	4.98	2.9	2.66	2.76	2.96
Ti	–	–	0.28	–	–	–	–	0.18	–	–
Al	4.02	2.01	1.56	1.20	1.05	4.01	2.01	1.68	1.24	1.04
Fe	0.86	2.43	1.30	–	–	0.81	0.18	1.13	–	–
Mn	0.01	0.04	–	–	–	0.01	0.11	–	–	–
Mg	1.14	0.57	0.95	–	–	1.18	0.53	1.19	–	–
Ca	–	0.05	–	0.18	–	–	0.06	–	0.22	–
Na	0.03	–	0.02	0.81	0.19	0.04	–	0.03	0.76	0.16
K	–	–	1.00	0.02	0.77	–	–	0.91	0.03	0.88
X_{Mg}	0.57		0.42			0.59				
X_{Na}				0.18					0.22	
X_{Alm}		0.76					0.73			
X_{Sps}		0.01					0.036			
X_{Prp}		0.14					0.17			
X_{Grs}		0.02					0.02			

<d.l. = less than detection limit; n.a. = not analyzed.

(Table 3). The diagnostic parameter (sigfit) seems to be better (0.31 against 0.52) for a higher CO_2 activity (X(CO2) = 0.5).

5. U/Pb geochronology

5.1. Methods

Zircons and monazites were separated by heavy liquids. All of the final mineral separates were obtained by hand-picking. To avoid any inherited grains, we choose to analyse monazite rather than zircon for two samples (MVG6 and MVG8).

Zircon and monazite were dissolved and analysed at the University of Clermont-Ferrand (UMR 6524, Magmas et Volcans) by ID–TIMS following the technique described by Paquette and Pin (2001). Total blanks were 2–5 pg for Pb. The U blanks were negligible. U and Pb isotopes were analysed on a Fison VG Sector 54–30 mass spectrometer in multi-collector static mode. Individual fraction ellipse errors (2σ) and regression calculations were determined using PbDat 1.24 and Isoplot/Ex 2.49 programs, respectively (Ludwig, 1993, 2001). The

Table 2
Whole-rock composition.

	MVG6	MVG8
SiO_2	62.60	74.91
TiO_2	0.98	0.08
Al_2O_3	18.54	13.67
FeO(total)	6.32	0.80
MnO	0.04	0.00
MgO	2.06	0.31
CaO	0.42	0.67
Na_2O	2.27	2.30
K_2O	5.94	6.11
P2O5	0.15	0.14
LOI	0.62	0.82
Total	99.94	99.81

uncertainties in ages are given at 95% confidence level. The decay constants used for the U–Pb system are those determined by Jaffrey et al. (1971) and advised by the IUGS (Steiger and Jäger, 1977).

5.2. U/Pb results

The zircon types from MVG2 (Fig. 2a) display a great heterogeneity and are usually metamict; they are mostly S-type according to the classification of Pupin (1976) and contain numerous inclusions. Zircons selected for dating are very elongate and thin euhedral (length > 10 × width), transparent, and colourless crystals. They do not show any inherited cores and have characteristics suggestive of a magmatic origin (Pupin, 1976).

Three fractions of zircon needles, (2, 3, and 5 grains) were analyzed from the leucogranite. Two zircon fractions were mechanically abraded according to the Krogh (1982) technique. These fractions have Pb and U concentration of 400–450 ppm and 9500–10,000 ppm, respectively. The contents of the unabraded zircon fraction are ten times lower (Table 4).

In a concordia diagram, these three fractions of highly elongate zircons define a discordia line, with an upper intercept of 318 ± 6 Ma and a lower intercept of −46 ± 66 Ma (MSWD = 0.52) (Fig. 6). The unabraded fraction shows a high degree of discordance, ~30%, most likely due to recent lead loss. Two euhedral single grains of monazite yield concordant points at 313 ± 1 Ma (Fig. 6). This age is in good agreement with the upper intercept zircon age of 318 ± 6 Ma. A discordia line can be defined by the three zircon fractions and the two monazite single grains with an upper intercept of 313 ± 4 Ma and a lower intercept of 0 ± 25 Ma (MSWD = 8). The weighted average of $^{207}Pb/^{206}Pb$ ages for these analytical points is 314 ± 4 Ma (MSWD = 6.4).

The upper intercept at 313 ± 4 Ma (Fig. 6) is interpreted as the age of syn-tectonic emplacement of the Pradines two-mica leucogranite because the analysed zircons likely had a magmatic origin and the
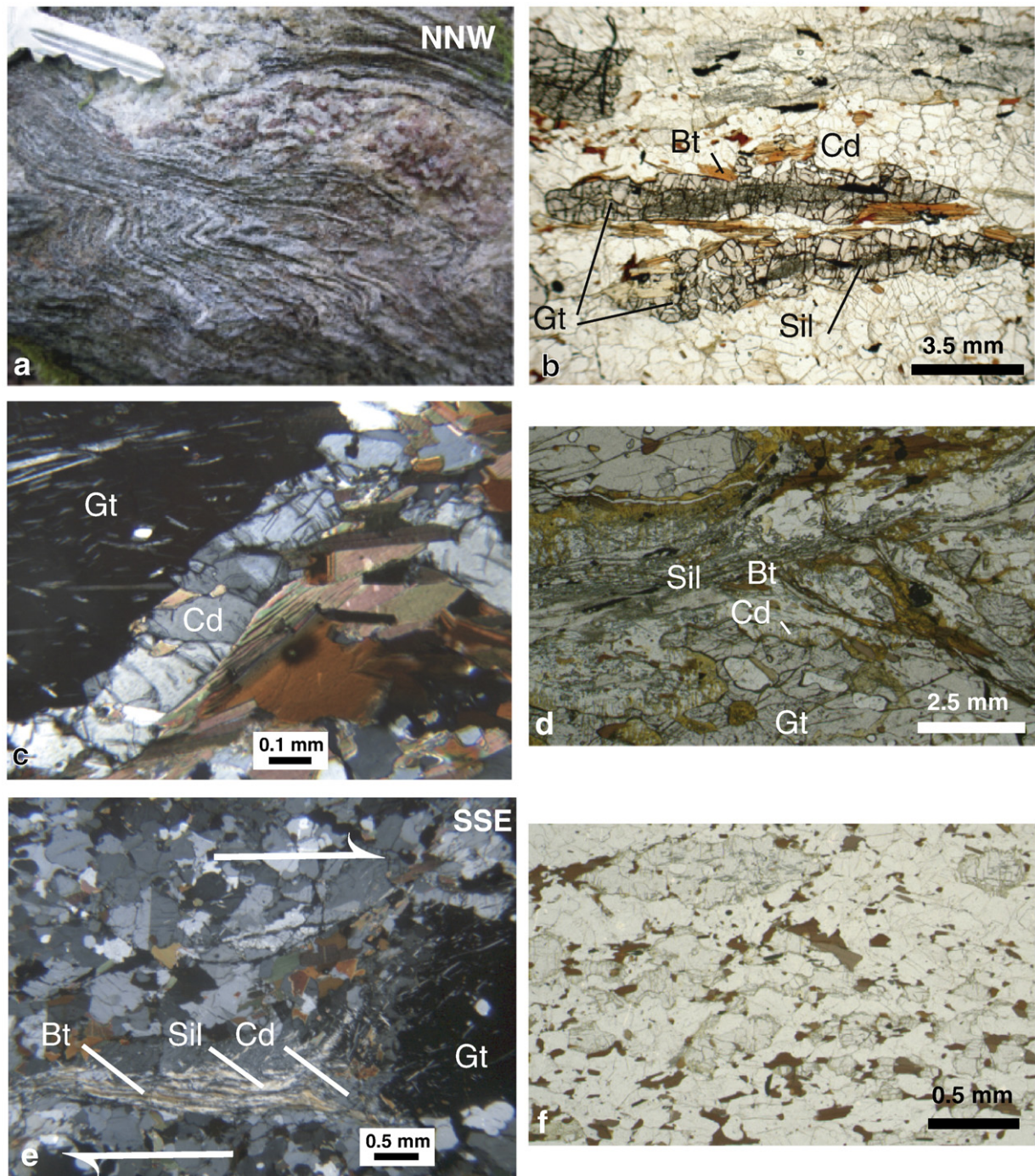
Fig. 4. (a) Microfolding of quartz aggregates and garnet ribbons indicating a dextral sense of shear for the Pradines shear zone. (b) Pancake-shaped garnets in the XZ plane with sillimanite inclusions in the core. (c) Cordierite reaction around garnet. (d) Garnet–cordierite–sillimanite–biotite assemblage. (e) Cordierite–sillimanite–biotite asymmetric pressure shadows around garnet, consistent with a dextral sense of shear. (f) Coarse-grained cordierite in a leucosome.

closure temperature for the monazite U/Pb system is estimated at ~600–750 °C (Copeland et al., 1988; Parrish, 1990).

In the high-grade migmatitic gneiss MVG6 (Fig. 2a), five monazite single grains were analyzed (Table 4). The Pb and U contents are 1500–6500 ppm and 14,500–70,000 ppm, respectively. In the concordia diagram, the five points are concordant to sub-concordant. The analytical point n°10 is interpreted to result from minor Pb loss (<1%). A linear regression of these five points gives an upper intercept age of 315 ± 4 Ma and 0 ± 25 Ma for the lower intercept (MSWD = 10.7) (Fig. 7a). The weighted average 207Pb/206Pb age is 315 ± 3 Ma.

In the high-grade migmatite leucosome sample MVG8 (Fig. 2a), five monazite single grains were analysed (Table 4). The Pb and U contents are heterogeneous: e.g. Pb contents range between 884 ppm and 20,088 ppm (Table 4). In the concordia diagram, the five points are concordant to sub-concordant around 313 and 320 Ma (Fig. 7b). The weighted average of the ^{206}Pb/^{238}U and ^{207}Pb/^{235}U ages are similar: 316 ± 2 Ma and 315.5 ± 2.2 Ma, respectively.

Both migmatitic gneiss samples give ages of around 315–316 Ma. Taking into account the high closure temperature for the monazite U/Pb system, these ages are interpreted as the minimum age of high-grade metamorphism (MVG6) and contemporaneous migmatization
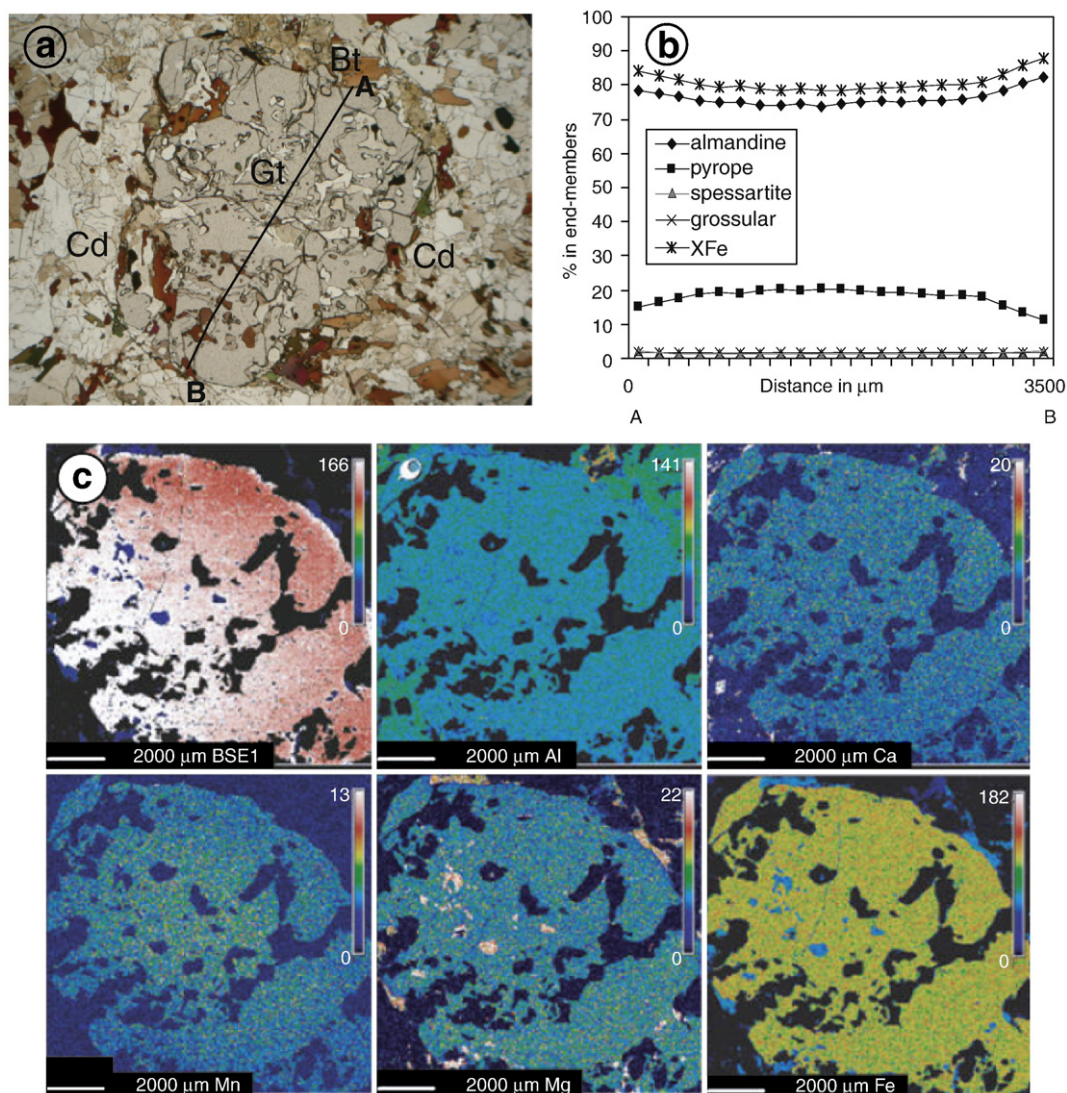
Fig. 5. Garnet from MVG6 (a) where compositional profile has been performed (b). (c) X-ray elements maps for Al, Ca, Mn, Mg and Fe of garnet from MVG8.

(MVG8). Collectively, the twelve monazites (Fig. 8a) coming from MVG2, MVG6 and MVG8 are concordant and range between 311 and 320 Ma with a weighted average $^{207}Pb/^{206}Pb$ of 315 ± 2 Ma (Fig. 8a and b).

6. Thermo-tectonic history of the Millevaches massif and comparison with the Velay dome

The range of $^{40}Ar/^{39}Ar$ ages between 303.0 ± 3.0 Ma, and 313.7 ± 3.1 Ma of the Pradines mylonitic granite (Gébelin et al., 2007) is consistent with the 313 ± 4 Ma U–Pb age. However, a precise evaluation of a cooling rate would be risky. Many granites of the Limousin region display similarities with the Millevaches granites: syntectonic peraluminous leucogranite bodies emplaced in the middle crust as laccoliths that subsequently experienced rapid cooling (Fig. 2a). During the time of syntectonic emplacement of the Millevaches granite (313 ± 4 Ma) within the dextral strike–slip Pradines shear zone, these leucogranites were also emplaced in the Limousin region which was still in transpression (Gébelin et al., 2007). The similar ages determined for the migmatitic gneiss may indicate that high-grade metamorphism, migmatization, and emplacement of the two-mica leucogranite (Fig. 8a and b) were also coeval with activity of the Pradines ductile shear zone.

Leucogranites with similar characteristics and age can be found elsewhere in the eastern part of the French Massif Central (Fig. 2a–b) and in the Variscan orogen in general (e.g. Bernard-Griffiths et al., 1985; Guineberteau et al., 1987; Fernandez-Suarez et al., 2000; Valle Aguado et al., 2005). Like the Millevaches massif, the Velay dome represents one of the largest granitic and migmatitic massif of the Variscan belt. It experienced leucogranite migmatization and magmatism at 314 ± 5 Ma and 301 ± 4 Ma, respectively (Fig. 2a–b; Mougeot et al., 1997). In contrast to the Millevaches massif, migmatization and magmatism in the Velay dome are two individual thermal events. Associated with larger laccoliths of leucogranites (Be Mezenne, 2005), emplacement of migmatites occurred within P–T conditions at ~700 °C–4 kbar (Montel et al., 1992) and emplacement is related to the development of south-verging thrust zones between 340 and 314 Ma (Ledru et al., 2001). The syntectonic emplacement of these migmatites (Burg and Vanderhaeghe, 1993; Ledru et al., 2001) implies that extensional events started to be active while the Variscan orogen was still under compression. The second phase of melting giving rise to the Velay granite (301 ± 4 Ma, Mougeot et al., 1997) is characterized by higher P–T conditions (~760–850 °C, 4.4–6.0 kbar, Montel et al., 1992) and is considered to be generally synchronous with emplacement of cordierite-bearing granites due to breakdown of hydrous mineral phases. This last thermal event is within the

Table 3
P–T conditions recorded by sample MVG6 and MVG8.

Sample	Independent set of reactions	Results
MVG6-garnet core	1) gr + q + 2sill = 3an 2) 2py + 5q + 4sill = 3crd 3) 5gr + 3fcrd + 6sill = 2 alm + 15an 4) py + east + 3q = phl + crd 5) east + 2crd = 2py + san + H$_2$O + 3sill 6) 4ann + 3fcrd + 3q = 6 alm + 4san + 4H$_2$O	For X(H$_2$O) = 1 T = 836 ± 57 °C P = 6.1 ± 0.8 kbar sigfit = 0.47 (1.61)

MVG6-garnet core	1) gr + q + 2sill = 3an
	2) 2py + 5q + 4sill = 3crd
	3) 2 alm + 6an + 3q = 2gr + 3fcrd
	4) 10phl + 21sill = 9east + san +
	    6 crd + H$_2$0
	5) 4ann + 3fcrd + 3q = 6 alm +
	    4san + 4H$_2$0
	6) 2gr + east + 2crd = py + phl + 6an
		For X(CO$_2$) = 0.2 and
		X(H$_2$O) = 0.8
		T = 810 ± 54 °C
		P = 5.7 ± 0.8 kbar
		sigfit = 0.45 (1.54)

MVG8-garnet core	1) 4ann + 3fcrd + 3q = 6 alm + 4san +
	    4H$_2$0
	2) py + phl + 6an = 2gr + east + 2crd
	3) py + 2gr + 3east + 6q = 3phl + 6an
	4) 7phl + 12an = 5py + 4gr + 3east +
	    4san + 4H$_2$0
	5) gr + 2ann + 3fcrd = 4 alm + 3an +
	    2san + 2H$_2$0
		For X(CO$_2$) = 0.1 and
		X(H$_2$O) = 0.9
		T = 805 ± 62 °C
		P = 6.1 ± 1.1 kbar
		sigfit = 0.52 (1.61)

MVG8-garnet core	1) 2 alm + 6an + 3q = 2gr + 3fcrd
	2) py + east + 3q = phl + crd
	3) 4ann + 3fcrd + 3q = 6 alm +
	    4san + 4H$_2$O
	4) py + phl + 6an = 2gr + east + 2crd
	5) 7phl + 12an = 5py + 4gr + 3east +
	    4san + 4 H$_2$O
		For X(CO$_2$) = 0.5 and
		X(H$_2$O) = 0.5
		T = 758 ± 53 °C
		P = 5 ± 1.1 kbar
		sigfit = 0.31 (1.61)

Abbreviations: alm = almandine; an = anorthite; ann = annite; crd = cordierite; east = eastonite; fcrd = Fe-cordierite; gr = garnet; phl = phlogopite; py = pyrope; q = quartz; san = sanidine; sill = sillimanite.

Fig. 6. U–Pb Concordia diagrams for zircons and monazites from the Pradines mylonitic two-mica leucogranite (MVG2).

uncertainty of the measurement coeval with granulite-facies metamorphism at 300 ± 20 Ma (Pin and Vielzeuf, 1983) and could reflect asthenospheric upwelling and intrusion of mantle-derived magmas at the base of the Variscan crust.

The mineralogical assemblages and P–T conditions deduced from gneisses of the Millevaches massif (§4 and Table 3; Samples MVG6 and MVG8, ~5–6 kbar, ~700–850 °C) are consistent with those acquired on

the granulitic paragneisses described and dated around 300 Ma by Pin and Vielzeuf (1983). Emplacement of leucogranites in the Limousin region could be related to this large thermal anomaly that originated in the upper mantle, as originally proposed by Capdevila et al. (1973), Vidal (1976) and Ledru et al. (2001). Asthenospheric upwelling could have been responsible for the temperature increase favouring melting of hydrous minerals at the origin of Millevaches leucogranites. However, this major thermal event which was recorded in the eastern part of the French Massif Central at 300 ± 20 Ma is now more precise and re-evaluated at 315 ± 4 Ma from our new data. The error bar of U/Pb age of the eastern part (300 ± 20 Ma) makes impossible to differentiate these two possible different events.

7. Exhumation and magmatism in transpression

The Pradines shear zone, which affected the Millevaches massif over a zone >5 km wide, is part of a large pop-up structure called the

Table 4
U–Pb zircon and monazite data.

Sample	Weight (mg)	Concentration (ppm)		^{206}Pb/^{204}Pb	^{207}Pb/^{235}U	±2σ %	^{206}Pb/^{238}U	±2σ %	Rho	^{207}Pb/^{206}Pb	±2σ %	Ages (Ma)			
		Pb	U									^{207}Pb/^{235}U	^{206}Pb/^{238}U	^{207}Pb/^{206}Pb	±2σ
MVG 2: Pradines mylonite															
1 - Mnz	0.005	2426	25 346	3577	0.36185	0.26	0.04989	0.25	0.97	0.05260	0.07	314	314	312	±2
2 - Mnz	0.006	1217	16 730	6486	0.35990	0.37	0.04956	0.37	0.98	0.05267	0.06	312	312	315	±1
3 - Zircon	0.001	52.6	1272	475	0.25104	2.78	0.03396	1.42	0.56	0.05361	2.30	227	215	355	±52
4 - Zircon	0.001	404	9576	2386	0.31855	0.31	0.04369	0.18	0.62	0.05289	0.24	281	276	324	±6
5 - Zircon	0.001	456	9563	2786	0.36176	0.29	0.04859	0.18	0.66	0.05399	0.21	314	306	371	±5
MVG 6: Mesosome															
6 - Mnz	0.010	1316	14 625	41 381	0.36542	0.36	0.05038	0.37	0.99	0.05260	0.05	316	317	312	±1
7 - Mnz	0.009	1387	15 007	28 848	0.36900	0.33	0.05076	0.33	0.98	0.05272	0.05	319	319	317	±1
8 - Mnz	0.002	2049	22 258	6594	0.36690	0.30	0.05048	0.22	0.78	0.05272	0.09	317	317	317	±2
9 - Mnz	0.002	6487	70 370	16 918	0.36387	0.36	0.05007	0.35	0.98	0.05270	0.07	315	315	316	±2
10 - Mnz	0.001	2139	22 501	6674	0.35892	0.27	0.04948	0.18	0.70	0.05261	0.19	311	311	312	±4
MVG 8: Leucosome															
11 - Mnz	0.003	4148	43 775	3398	0.36329	0.32	0.05018	0.32	0.97	0.05251	0.07	315	316	308	±2
12 - Mnz	0.006	1093	8588	2988	0.36494	0.35	0.05033	0.31	0.89	0.05258	0.16	317	316	311	±4
13 - Mnz	0.004	884	6866	3757	0.36422	0.40	0.05028	0.25	0.67	0.05253	0.29	316	315	309	±7
14 - Mnz	0.003	2815	21 037	1422	0.36220	0.32	0.04996	0.26	0.86	0.05258	0.16	314	314	311	±4
15 - Mnz	0.006	20 088	19 037	2179	0.36830	0.36	0.05074	0.33	0.91	0.05264	0.14	318	319	313	±3

Isotopic ratios are corrected for mass discrimination (0.1%/amu for Pb and U), isotopic tracer contribution and blanks. Initial common Pb is determined using the Stacey and Kramers (1975) two-step model. The errors on the isotope ratios are quoted in %.
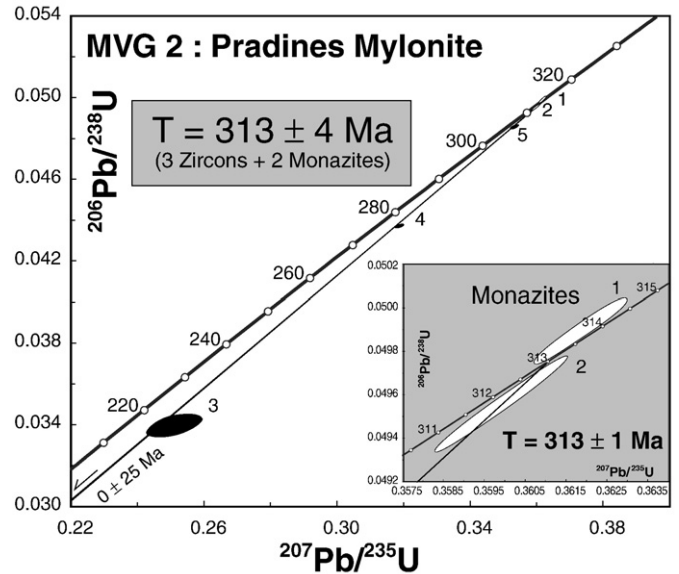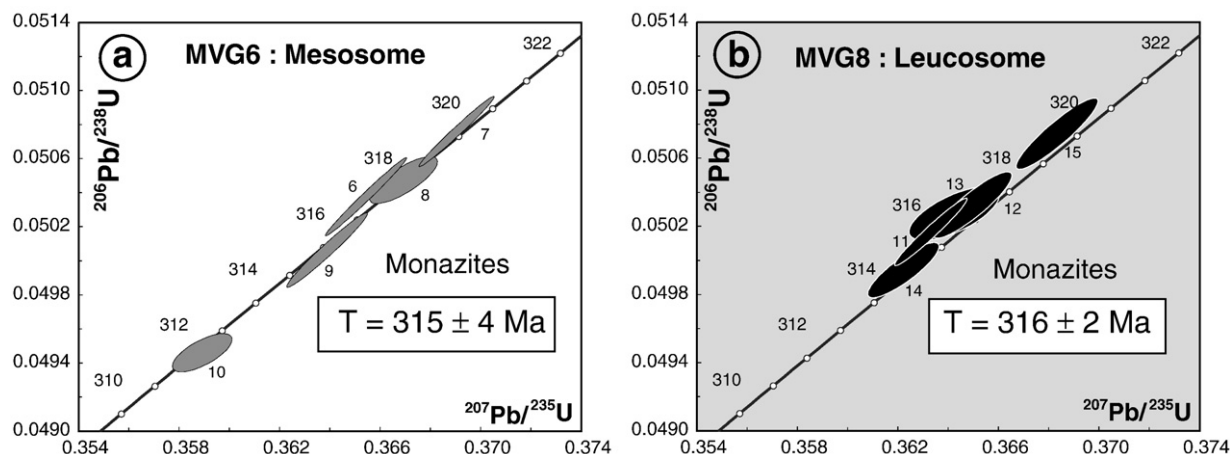
Fig. 7. U–Pb Concordia diagrams from the high grade metamorphic rocks: (a) a migmatite mesosome (MVG 6) and (b) a migmatite leucosome (MVG 8).

South Armorican Limousin Shear Zone (SALSZ; Fig. 1b) that extends from the Armorican Massif to the Limousin area (Gébelin et al., 2007). To the south, major left-lateral ductile shear zones in the Galician region (Spain; Fig. 1a) also host Variscan syntectonic granites that are similar in age, composition and structure to those in the Armorican Massif and the Massif Central (Ortega and Ibarguchi, 1990; Fernandez-Suarez et al., 2000; Valle Aguado et al., 2005). The Galician region, in the western end of the Ibero–Armorican tectonic arcs, exhibits major left-lateral ductile shear zones which can be interpreted as conjugate structures to the SALSZ (Fig. 1a–b). With its 1700 km length, this pop-up structure, active from 350 to 300 Ma (Gébelin, 2004), is similar in magnitude to the largest SE Asian intracontinental faults.

7.1. Importance of strike–slip shear zones during exhumation

Comparable studies in central Anatolia (Umhoefer et al., 2007; Whitney et al., 2007), Namibia (Goscombe et al., 2003), East Antarctica (Pelletier et al., 2002) and SE Asia (Leloup et al., 1995; Chetty and Bhaskar Rao, 2006) have shown that such intracontinental strike–slip shear zones play a significant role in the exhumation of orogenic crust. For example in SE Asia, high-grade metamorphic rocks (domes) occur in the Red River shear zone (Leloup et al., 2001). The large magnitude of inferred ductile strain and left-lateral offset along the Red River shear zone suggest that it played a major role in the exhumation of high-grade metamorphic rocks, perhaps by small

deviations in the shear direction from the horizontal that induced local vertical movement (Tapponnier et al., 1990). Therefore, intra-continental strike–slip faulting can induce lateral (>100's–1000 km) and vertical displacement (~10–20 km), the latter of which becomes significant in the thermal and rheological evolution of continental crust. As shown by studies of intracontinental strike–slip faults and exhumed orogenic crust, there is a spatial and temporal relationship between the transpressional regime, crustal melting (e.g. migmatiza-tion and formation of leucogranite), rapid exhumation and cooling of high-grade metamorphic rocks, and ascent of magma (Leloup et al., 1995; Fritz et al., 1996; Whitney et al., 2003, 2007).

In the case of the Millevaches Massif, granites, high-grade meta-morphic rocks and micaschists display a foliation which strikes NNW–SSE, and dips steeply (>55°), with a lineation that range between 0 and 30°. As outlined above shear sense indicators (C–S, asymmetric tails, shear bands) indicate a dextral wrench movement (Fig. 3b–c). The local variations of lineation plunges (from 0 to 30°) could have created small deviations in the shear direction helping some deep crustal rocks to be exhumed. At the scale of the Limousin region, the dominant strike–slip component is dextral with local occurrences of down–dip lineation and sinistral strike–slip kinematics. Collectively, these two observations are consistent with a component of coaxial deformation, vertical stretching direction in an overall transpressive system. The combination of coaxial and noncoaxial deformation, compatible with transpression (Gébelin et al., 2007), could have triggered the exhumation of the deep crustal rocks currently observed in the region.
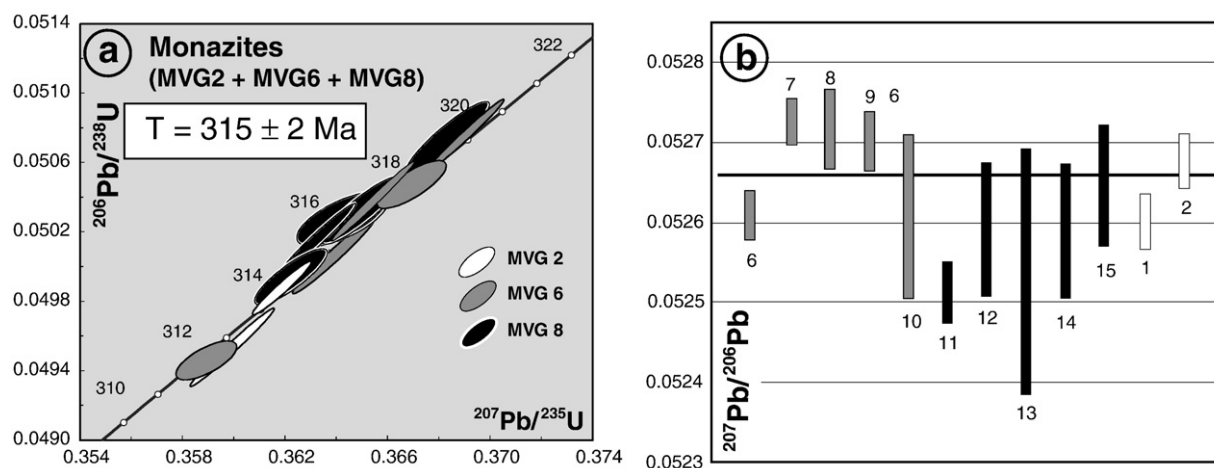

Fig. 8. U–Pb Concordia diagram samples (a) of twelve monazites from MVG2, MVG6 and MVG8 and (b) plot for the weighted average 207Pb/206Pb ratio. The mean age is 315 ± 2 Ma.

7.2. Exhumation in the Variscan transpressional regime: relationship between detachment zones, strike–slip shear zones and melt production

In the Variscan belt of Western Europe, the onset of syn-orogenic extension is estimated at 335 Ma by the so-called "Tuffs Anthracifères" that correspond to a magmatic event characterized by the emplacement of "red granites", granophyres and sub-aerial acidic volcanic rocks (Faure et al., 2002). However, the new data presented here confirm that the orogen was still in transpression at ca. 315 Ma (this study and Gébelin et al., 2007). Although emplaced within a strike–slip shear zone system, some syntectonic granites of the Limousin region are bounded at their roof by detachment zones (Figs. 2a–9). ^{40}Ar/^{39}Ar geochronology of single biotite grains from the N–S oriented normal-sense shear zones of the Brâme massif (Fig. 2a) yields a plateau age at 313 ± 3 Ma (Gébelin, 2004). This age, interpreted as a cooling age postdating high-temperature normal faulting marked by biotite and sillimanite shear bands, is coeval with Pradines wrench fault activity (Gébelin, 2004). Limiting the Millevaches massif to the west, the Argentat shear zone (Fig. 2a) can be described as a detachment zone similar to that limiting the Brâme massif. Indeed, clay particles coming from the Bosmoreau sedimentary basin, located in the Argentat hanging-wall, give an age of 296.5 ± 3.5 Ma (K-Ar method, Bruguier et al., 2003) that reflects the last stage of the Argentat detachment zone activity.

These low angle normal shear zones, which are perpendicular to the overall E–W trend of the orogen, may be related to orogenic collapse while the SALSZ was still active (Figs. 1 and 9). Similar to what Pin and Vielzeuf (1983) and Ledru et al. (2001) proposed for the east part of the French Massif Central, our data is consistent with the collapse of the Variscan belt coeval with widespread emplacement of granites and granulite facies rocks due to asthenospheric upwelling and associated intrusion of mantle-derived magmas at the base of the crust. Slab break off or thermal erosion of the lithospheric root of the Variscan belt (Rey et al., 1997) could be the underlying mechanism(s) that account for such a thermal anomaly in the crust. Whatever the origin of the heat source, one of the questions is to better understand the relationship between orogenic collapse and melt production while the orogen was still in transpression. The presence of granitic magma could have provided a low-viscosity zone that facilitated orogenic collapse. Teyssier et al. (2008) demonstrated that once an orogenic
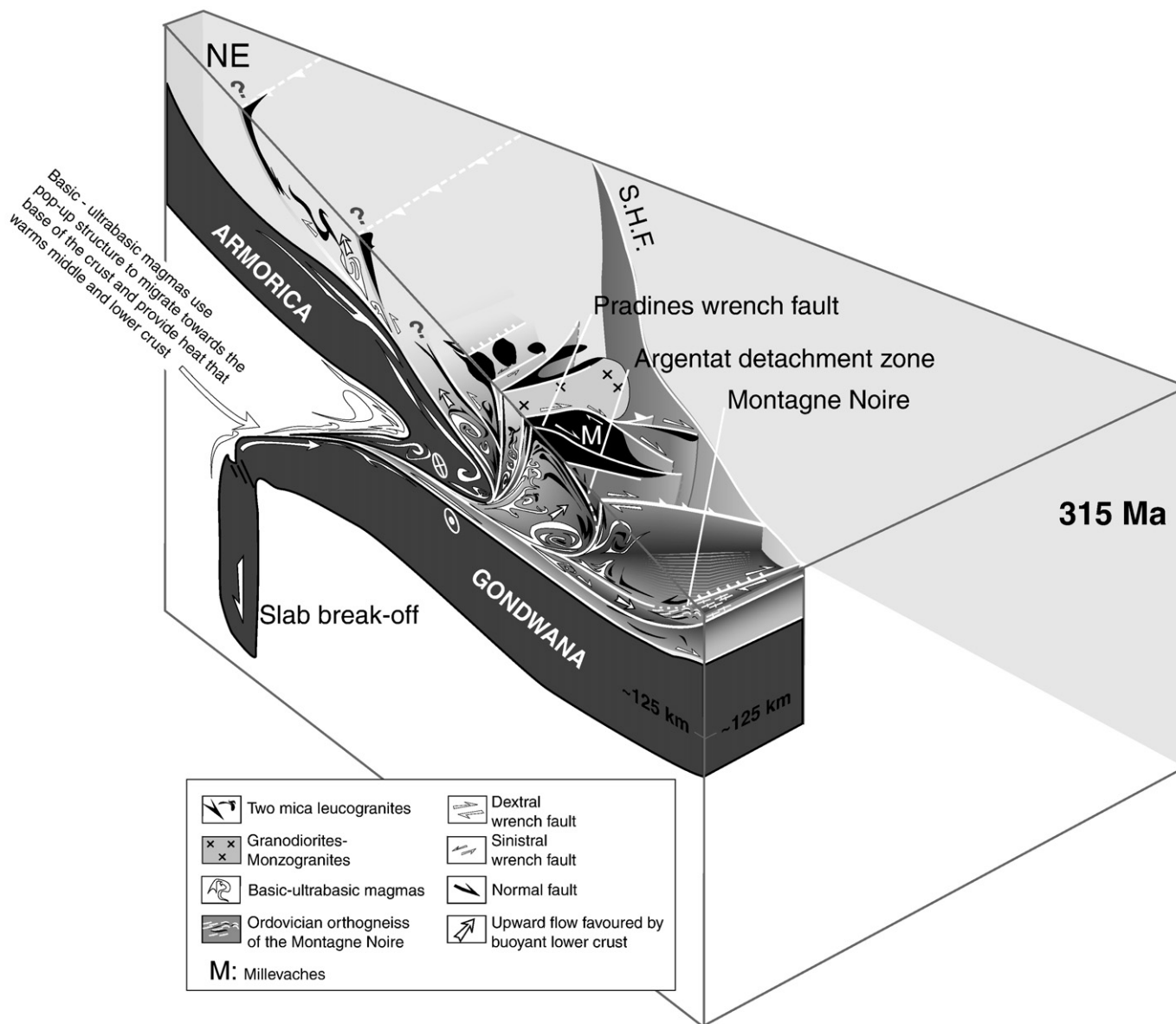

Fig. 9. Structural block-diagram of the Limousin region at around 315 Ma illustrating Variscan orogenic collapse in the internal zones while the system was still in transpression due to continued convergence between Gondwana and Laurentia–Baltica plates. (See text for explanations). S.H.F.: Sillon Houiller fault.

plateau has reached a critical thickness and thermal structure (the case for the Variscan belt at ~315 Ma), it flows under its own weight even with far-field contraction (continued plate convergence). Their modelling shows that foreland regions and orogenic plateau can have coeval contraction and extension dynamics that are not readily related to boundary velocities. Whatever the boundary conditions (fixed, slow or fast extension boundary), in the presence of buoyant lower crust, extension in the plateau is enhanced that in turn allows shortening of foreland regions. Indeed, when an extensional velocity is applied at the model boundary, thrust faulting in the foreland is still activated because the gravitational flow velocity exceeds the extension velocity. The models presented in Teyssier et al. (2008) show that if extension is slow, buoyant lower crust favours upward flow into metamorphic core complex rather than extrusion channel and when extension becomes faster (last orogenic stage), flow of plateau channel into metamorphic core complex is enhanced even if buoyancy is turned off.

Based on the new geochronological, metamorphic and structural data presented here, we propose that around 315 Ma, the Variscan orogen collapsed under its own weight, inducing the development of normal faults in the center of the pop-up structure and thrust faults (Gébelin et al., 2007) at the front of the collapsed zone (Fig. 9). In agreement with the model of Ledru et al. (2001) and Williamson et al. (1996), the heat source causing voluminous partial melting of the Variscan crust was supplied by asthenospheric upwelling and associated intrusion of mantle-derived magmas at the base of the crust (Fig. 9) that may have been enhanced by internal (radioactive) heat production of the overthickened crust in this part of the orogen (Lucazeau and Vasseur, 1981; Cuney et al., 1990). We propose that adjacent to the subduction zone, the pop-up structure may have facilitated the migration of basic magmas at the base of the crust warming the middle to lower crust and giving rise to partial melting reactions (Fig. 9). Strike–slip shear zones channeled magmas at depth, which once trapped in the middle crust, migrated into the pre-existent subhorizontal micaschist foliation (Gébelin et al., 2006). Some of these shear zones are also responsible for Sb–Au deposits in the upper crust (Bellot et al., 2003). At the same time, following the model of Teyssier et al. (2008), buoyant lower crust favours upward flow inducing development of detachment zones at the roof of the granite bodies (Fig. 9). The combination of the activation of strike–slip faulting with local variations of lineation dips (0 to 30°), detachment zones at the roof of syntectonic granites, and erosion may explain the exhumation of high-grade metamorphic, deep crustal rocks in the Limousin region.

The formation of the Montagne Noire gneiss dome, located in the southernmost part on the French Massif Central (Fig. 2a), could be a consequence of this contraction/extension system (Fig. 9). The Montagne Noire axial zone is interpreted to be the core of a anticlinal nappe stack (Matte et al., 1998). It consists of a high-grade metamorphic dome (Thompson and Bard, 1982) that forms a double antiform of paragneiss and orthogneiss derived from pre-Variscan Ordovician granites (Roger et al., 2004). The compressional event giving rise to the post-nappe anticline has been dated stratigraphically at 325 Ma (Engel et al., 1980). Syn-anatectic extensional events have been recognized in the Montagne Noire axial zone (Brunel and Lansigu, 1997) and are contemporaneous with the emplacement of the Vialais granite (Fig. 2a) dated at 327 ± 5 Ma (Matte et al., 1998). Normal faulting and wrenching at between 297 ± 3 Ma and 311 ± 4 Ma (Maluski et al., 1991) were responsible for the final dome emplacement. In conjunction, all of these ages associated with compressional or extensional events are consistent with those recorded in the Limousin region (Fig. 2a–b).

The Variscan "hot orogen" can be compared to various orogenic belts such as the Canadian Cordillera, the Tibetan plateau or the Aegean region. All of them are characterized by crustal thickening, thermal maturation, partial melting and syn- to post-convergence gravitational collapse. Asthenospheric upwelling associated with slab

break-off and radioactive decay are usually evoked as potential heat sources for partial melting of orogenic crust. In the case of the Variscan belt, two main parameters seemed to strongly control the evolution of orogenic crust: 1) heat production at the base of the crust inducing a buoyant lower crust that favors upward flow (Teyssier et al., 2008) and 2) shear zone activity: strike–slip localizes the flow by channeling the magma from depth to the middle crust and detachment zones accommodate magma emplacement. The previously-formed flat-lying micaschist foliation formed during nappe tectonics acts as a mechanical anisotropy of the middle crust that can also play a major role for magma emplacement that in turn controls the tectonic evolution.

Acknowledgements

References

Ait Malek, H., 1997. Pétrologie, géochimie et géochronologie U/Pb d'associations acide-basiques: exemples du SE du Velay (Massif Central français) et de l'anti-Atlas occidental (Maroc). Thèse doctorat, Univ. Nancy, 297pp.

Alexandrov, P., Cheilletz, A., Deloule, E., Cuney, M., 2000. 319 ± 7 Ma age for the blond granite (northwest Limousin, French Massif Central) obtained by U–Pb ion-probe dating of zircons. C.R. Acad. Sci. Paris 330, 1–7.

Arthaud, F., Matte, P., 1977. Late-Paleozoic strike–slip faulting in southern Europe and northern Africa: result of a right lateral shear zone between the Appalachians and the Urals. Geol. Soc. Amer. Bull. 88, 1305–1320.

Audrain, J., Vigneresse, J.L., Cuney, M., Friedrich, M., 1989. Modèle gravimétrique et mise en place du complexe granitique hyperalumineux de St Sylvestre (Massif Central français). C.R. Acad. Sci. Paris 309, 1907–1914.

Bellot, J.P., Lerouge, C., Bailly, L., Bouchot, V., 2003. The Biards Sb–Au — bearing shear zone (Massif Central, France): an indicator of crustal-scale transcurrent tectonics guiding Late Variscan collapse. Econ. Geol. 98, 1427–1447.

Be Mezeme, E., 2005. Contribution de la géochronologie U–Th–Pb sur monazite à la compréhension de la fusion crustale dans la chaîne varisque française et implication géodynamique. Thèse doctorat, Univ. d'Orléans.

Bernard-Griffiths, J., Peucat, J.J., Sheppart, S., Vidal, P., 1985. Petrogenesis of Hercynian leucogranites from the southern Armorican Massif: contribution of REE and isotopic (Sr, Nb, Pb and O) geochemical data to the study of source rock characteristics and ages. Earth Planet. Sci. Lett. 74, 235–250.

Bertrand, J.M., Leterrier, J., Cuney, M., Brouand, M., Stussi, J.M., Delaperierre, E., Virlogieux, E., 2001. Géochronologie U–Pb sur zircons de granitoïdes du Confolentais, du massif de Charroux-Civray (seuil du Poitou) et de Vendée. Geol. France 167–181.

Binon, M., Pin, C., 1989. Géochronologie Rb–Sr et U–Pb des granites du Mayet-de-Montagne et des Bois Noirs, Montagne bourbonnaise (Massif Central). Bull. Soc. Géol. Fr. 4, 695–703.

Brichau, S., Respaut, J.P., Monié, P., 2008. New age constraints on emplacement of the cevenol granitoids, south French Massif Central. Int. J. Earth Sci. 97, 725–738.

Burg, J.P., Vanderhaeghe, O., 1993. Structures and way-up criteria in migmatites, with application to the Velay dome (French Massif central). J. Struct. Geol. 15, 1293–1301.

Burg, J.P., Brun, J.P., Van Den Driesche, J., 1990. Le sillon houiller du Massif Central Français: faille de transfert pendant l'amincissement crustal de la chaine varisque? C.R. Acad. Sci. Paris 311, 147–152.

Burg, J.P., Leyreloup, A., Marchand, J., Matte, P., 1984. Inverted metamorphic zonation and large scale thrusting in Variscan Belt: an example in the French Massif central. In: Hutton, D.H.W., Sanderson, D.J. (Eds.), Variscan Tectonics of the North Atlantic Region. Geol. Soc. Spec. Publ. London, vol. 14, pp. 44–61.

Brown, M., 2004. The mechanism of melt extraction from lower continental crust of orogens. Trans. R. Soc. Edinb. Earth Sci. 95, 35–48.

Brown, M., Dallmeyer, D., 1996. Rapid Variscan exhumation and the role of magma in core complex formation: southern Brittany metamorphic belt, France. J. Metamorph. Geol. 14, 361–379.

Bruguier, O., Becq-Giraudon, J.F., Clauer, N., Maluski, H., 2003. From Late Visean to Stephanian: pinpointing a two-stage basinal evolution in the Variscan belt. A case study from the Bosmoreau Basin (French Massif Central) and its geodynamic implications. Int. J. Earth Sci. 92, 338–347.

Brunel, M., Lansigu, C., 1997. Déformation et cinématique de mise en place du dôme de la zone axiale de la Montagne Noire: signification des nodules à quartz–sillimanite (Massif central français). C.R. Acad. Sci. Paris 325, 517–523.

Capdevila, R., Corretgé, G., Floor, P., 1973. Les granitoides varisques de la Meseta ibérique. Bull. Soc. Géol. Fr. XV, 209–228.

Cheilletz, A., Archibald, D.A., Cuney, M., Charoy, B., 1992. Ages ^{39}Ar/^{40}Ar du leucogranite à topaze–lépidolite de Beauvoir et des pegmatites sodomithiques de Chédeville (Nord du Massif Central, France). Signification pétrologique et géodynamique. C.R. Acad. Sci. Paris 305, 1167–1173.

Chetty, T.R.K., Bhaskar Rao, Y.J., 2006. Constrictive deformation in transpressional regime: field evidence from the Cauvery Shear Zone, Southern Granulite Terrain, India. J. Struct. Geol. 28, 713–720.

Choukroune, P., Gapais, D., Matte, P., 1983. Tectonique hercynienne et déformation cisaillante: la faille ductile senestre de la Marche (Massif Central Français). C.R. Acad. Sci. Paris 296, 859–862.

Copeland, P., Parrish, R.R., Harrison, T.M., 1988. Identification of inherited Pb in monazite and its implications for U–Pb systematics. Nature 333, 760–763.

Cuney, M., Friedrich, M., Blumenfeld, P., Bourguignon, A., Boiron, M.C., Vigneresse, J.L., Poty, B., 1990. Metallogenesis in the French part of the Variscan orogen. Part I: U preconcentrations in pre-Variscan and Variscan formations — a comparison with Sn, W and Au. Tectonophysics 177, 39–57.

Downes, H., Dupuy, C., Leyreloup, A.F., 1990. Crustal evolution of the Hercynian belt of Western Europe: evidence from lower crustal granulitic xenoliths (French Massif Central). Chem. Geol. 83, 209–231.

Dumas, E., Faure, M., Pons, J., 1990. L'architecture des plutons leucogranitiques du plateau d'Aigurande et l'amincissement crustal tardi-Varisque. C.R. Acad. Sci. Paris 310, 1533–1539.

Echtler, H., Malavieille, J., 1990. Extensional tectonics, basement uplift and Stephano–Permian collapse basin in a Late Variscan metamorphic core complex (Montagne Noire, southern Massif Central). Tectonophysics 177, 125–138.

Engel, W., Feist, R., Franke, W., 1980. Le Carbonifère anté-stéphanien de la Montagne Noire: rapports entre mise en place des nappes et sédimentation. Bull. BRGM 4, 341–389 sect. I.

Faure, M., 1989. L'amincissement crustal de la chaine varisque à partir de la déformation ductile des leucogranites du Limousin. C.R. Acad. Sci. Paris 309, 1839–1845.

Faure, M., 1995. Late Carboniferous extension in the Variscan French Massif Central. Tectonics 14, 132–153.

Faure, M., Pons, J., 1991. Crustal thinning recorded by the shape of the Namurian–Wesphalian leucogranite in the Variscan Belt of the northwest Massif Central, France. Geology 19, 730–733.

Faure, M., Prost, A., Lasne, E., 1990. Déformation ductile extensive d'âge Namuro–Wesphalien dans le plateau d'Aigurande, Massif Central Français. Bull. Soc. Géol. Fr. 8, 189–197.

Faure, M., Leloix, C., Roig, J.Y., 1997. L'évolution polycyclique de la chaîne hercynienne. Bull. Soc. Géol. Fr. 168, 695–705.

Faure, M., Monié, P., Pin, C., Maluski, H., Leloix, C., 2002. Late Visean thermal event in the northern part of the French Massif Central: new ^{40}Ar/^{39}Ar and Rb–Sr isotopic constraints on the Hercynian syn-orogenic extension. Int. J. Earth Sci. 91, 53–75.

Fernández-Suárez, J., Dunning, G.R., Jenner, G.A., Gutiérrez Alonso, G., 2000. Variscan collisional magmatism and deformation in NW Iberia: constraints from U–Pb geochronology of granitoids. J. Geol. Soc. Lond. 157, 565–576.

Fritz, H., Wallbrecher, E., Khudeir, A.A., Abu El Ela, F., Dallmeyer, D.R., 1996. Formation of Neoproterozoic metamorphic core complexes during oblique convergence (Eastern Desert, Egypt). J. Afr. Earth Sci. 23, 311–329.

Gapais, D., Lagarde, J.L., Le Corre, C., Audren, C., Jegouzo, P., Casas Sainz, A., Van den Driessche, J., 1993. La zone de cisaillement de Quiberon: témoin d'extension de la chaîne varisque en Bretagne méridionale au Carbonifère. C.R. Acad. Sci. Paris 316, 1123–1129.

Gébelin, A., 2004. Déformation et mise en place des granites (360–300Ma) dans un segment de la Chaine Varisque (Plateau de Millevaches, Massif Central), Ph.D., Univ. Montpellier II, Montpellier, France, 235 pp.

Gébelin, A., Martelet, G., Brunel, M., Faure, M., Rossi, P., 2004. Late Hercynian leucogranites modelling as deduced from new gravity data: the example of the Millevaches massif, Massif Central, France. Bull. Soc. Géol. Fr. 175, 239–248.

Gébelin, A., Martelet, G., Chen, Y., Brunel, M., Faure, M., 2006. Structure of Late Variscan Millevaches leucogranite massif in the French Massif Central: AMS and gravity modelling results. J. Struct. Geol. 28, 148–169.

Gébelin, A., Brunel, M., Monié, P., Faure, M., Arnaud, N., 2007. Transpressional tectonics and carboniferous magmatism in the Limousin, Massif Central, France: structural and ^{40}Ar/^{39}Ar investigations. Tectonics 26, TC2008. doi:10.1029/2005TC001822.

Gilotti, J.A., Elvevold, S., 2002. Extensional exhumation of a high-pressure granulite terrane in Payer Land, Greenland Caledonides: structural, petrologic and geochronologic evidence from metapelites. Can. J. Earth Sci. 39, 1169–1187.

Godin, L., Grujic, D., Law, R.D., Searle, M.P., 2006. Channel flow, ductile extrusion and exhumation in continental collision zones: an introduction. Channel Flow, Ductile Extrusion and Exhumation in Continental Collision Zones. Geol. Soc. London, Spec. Publ., vol. 268, pp. 1–23.

Goscombe, B., Hand, M., Gray, G., Mawby, J., 2003. The metamorphic architecture of a transpressional orogen: the Kaoka Belt, Namibia. J. Petrol. 44, 679–711.

Groome, W.G., Koons, P.O., Johnson, S.E., 2008. Metamorphism, transcient mid-crustal rheology, strain localization and the exhumation of high-grade metamorphic rocks. Tectonics 27, TC1001. doi:10.1029/2006TC001992.

Guineberteau, B., Bouchez, J.L., Vigneresse, J.L., 1987. The Mortagne granite pluton (France) emplaced by pull apart along a shear zone: structural and gravimetric arguments and regional implication. Geol. Soc. Amer. Bull. 99, 763–770.

Hodges, K.V., 2006. A synthesis of the channel flow — extrusion hypothesis as developed for the Himalayan–Tibetan orogenic system. Channel Flow, Ductile Extrusion and Exhumation in Continental Collision Zones. Geol. Soc., London, Spec. Publ., vol. 268, pp. 71–90.

Holland, T.J.B., Powell, R., 1998. An internally-consistent thermodynamic data set for phases of petrologic interest. J. Metamorph. Geol. 16, 309–343.

Holliger, P., Cuney, M., Friedrich, M., Turpin, L., 1986. Age carbonifère de l'Unité de Brâme du complexe granitique peralumineux de St Sylvestre (NW du Massif Central) défini par les données isotopiques U–Pb sur zircon et monazite. C.R. Acad. Sci. Paris 303, 1309–1314.

Isnard, H., 1996. Datation par la méthode U–Pb sur monazites des granites du Mont Lozère et de l'Est de la Margeride (laccolites de Chambon-le-Château et de St-Christophe d'Allier): contribution à l'histoire post-tectonique du Massif Central Français. Master thesis, Univ. Montpellier II, Montpellier, 55pp.

Jaffrey, A.H., Flynn, K.F., Glendenin, L.E., Bentley, W.C., Essling, A.M., 1971. Precision measurement of half-lives and specific activities of 235U and 238U. Phys. Rev. C4, 889–1906.

Johnson, T., Brown, M., 2004. Quantitative constraints on metamorphism in the Variscides of Southern Brittany — a complementary pseudosection approach. J. Petrol. 45, 1237–1259.

Krogh, T.E., 1982. Improved accuracy of U–Pb zircon ages by the creation of more concordant systems using air abrasion technique. Geochim. Cosmochim. Acta 46, 637–649.

Lafon, J.M., Respaut, J.P., 1988. Géochronologie U–Pb et leucogranites varisques: cas des massifs de Grandrieu et de la Porcherie (Limousin), Massif Central Français. Bull. Min. 111, 225–237.

Lameyre, J., 1984. Contribution à la géologie du Limousin; (II), les leucogranites fini-carboniferes et le modele himalayen. C.R. Acad. Sci. Paris 298, 895–900.

Lardeaux, J.-M., Ledru, P., Daniel, I., Duchêne, S., 2001. The Variscan French Massif Central: a new addition to the ultra-high pressure metamorphic 'club': exhumation processes and geodynamic consequences. Tectonophysics 332, 143–167.

Le Breton, N., Thompson, A.B., 1988. Fluid-absent (dehydration) melting of biotite in metapelites in the early stages of crustal anatexis. Contrib. Mineral. Petrol. 99, 226–237.

Le Carlier de Veslud, C., Cuney, M., Royer, J.J., Floc'h, J.P., Ameglio, L., Alexandrov, P., Vigneresse, J.L., Chevremont, P., Itard, Y., 2000. Relationships between granitoids and mineral deposits: three-dimensional modelling of the Variscan Limousin Province (NW French Massif Central). Trans. R. Soc. Edinb. Earth Sci. 91, 283–301.

Ledru, P., Autran, A., 1987. L'édification de la chaîne varisque dans le Limousin. Rôle de la faille d'Argentat à la limite Limousin-Millevaches. Doc. BRGM 140, 51–81.

Ledru, P., Lardeaux, J.M., Santallier, D., Autran, A., Quenardel, J.M., Floc'h, J.P., Lerouge, G., Maillet, N., Marchand, J., Ploquin, A., 1989. Où sont les nappes dans le Massif Central français ? Bull. Soc. Géol. Fr. 8, 605–618.

Ledru, P., Autran, A., Santallier, D., 1994. Lithostratigraphy of Variscan terranes in the French Massif Central: a basis for paleogeographical reconstitution. In: Keppie, J.D. (Ed.), Pre-Mesozoic Geology in France and Related Areas. Springer, New York, pp. 276–288.

Ledru, P., Courrioux, G., Dallain, C., Lardeaux, J.M., Montel, J.M., Vanderhaeghe, O., Vitef, G., 2001. The Velay dome (French Massif Central): melt generation and granite emplacement during orogenic evolution. Tectonophysics 342, 207–237.

Leloup, P.H., Lacassin, R., Tapponnier, P., Scharrer, U., Dailai, Z., Xiaohan, L., Liangshang, Z., Trinh, P.T., 1995. The Ailao Shan–Red River shear zone (Yunnan, China), Tertiary transform boundary of Indochina. Tectonophysics 251, 3–84.

Leloup, P.H., Arnaud, N., Lacassin, R., Kienast, J.R., Harrison, T.M., Phan, Trong Trinh, Replumaz, A., Tapponnier, P., 2001. New constraints on the structure, thermo-chronology and timing of the Ailao Shan — Red River shear zone, SE Asia. J. Geophys. Res. 106, 6657–6671.

Liu, M., Shen, Y., 1998. Crustal collapse, mantle upwelling, and Cenozoic extension in the North America Cordillera. Tectonics 17, 311–321.

Lucazeau, F., Vasseur, G., 1981. Production de chaleur et régime thermique de la croute du Massif Central. Ann. Geophys. 37, 493–513.

Ludwig, K.R., 1993. Pbdat: A Computer Program for Processing Pb–U–Th isotope Data, Version 1.24. U. S. Geol. Surv. Open-File Rep, pp. 88–542.

Ludwig, K.R., 2001. User Manual for Isoplot/Ex rev. 2.49. A Geochronological Toolkit for Microsoft Excel. Berkeley Geochronology Center Spec. Publ., vol. 1a, pp. 1–56.

Maluski, H., Costa, S., Echtler, H., 1991. Late Variscan tectonic evolution by thinning of earlier thickened crust. An ^{40}Ar–^{39}Ar study of the Montagne Noire, southern Massif Central, France. Lithos 26, 287–304.

Martínez-Martínez, J.M., Soto, J.I., Balanyá, J.C., 2004. Elongated domes in extended orogens: a mode of mountain uplift in the Betics (SE Spain). In: Whitney, D.L., Teyssier, C., Siddoway, C.S. (Eds.), Gneiss Domes in Orogeny, Geol. Soc. Am. Spec. Publ., vol. 380, pp. 243–265.

Mattauer, M., Brunel, M., Matte, P., 1988. Failles normales ductiles et grands chevauchements: une nouvelle analogie entre l'Himalaya et la chaine hercynienne du Massif Central Français. C.R. Acad. Sci. Paris 306, 671–676.

Matte, P., 1986. Tectonics and plate tectonics model for the Variscan Belt of Europe. Tectonophysics 126, 329–374.

Matte, P., 1991. Accretionary history and crustal evolution of the Variscan Belt in western Europe. Tectonophysics 196, 309–339.

Matte, P., 2002. Variscides between the Appalachians and the Urals: similarities and differences between Paleozoic subduction and collision belts. Geol. Soc. Am. Bull. 364, 239–251.

Matte, P., Lancelot, J., Mattauer, M., 1998. La zone axiale hercynienne de la Montagne noire n'est pas un « metamorphic core complex » extensive mais un anticlinal post-nappe à coeur anatectique. Geodin. Acta 11, 13–22.

Meissner, R., Mooney, W., 1998. Weakness of the lower continental crust: a condition for delamination, uplift, and escape. Tectonophysics 296, 47–60.

Ménard, G., Molnar, P., 1988. Collapse of a Hercynian Tibetan Plateau into a Late Paleozoic European Basin — and — Range province. Nature 334, 235–237.

Mercier, L., Johan, V., Lardeaux, J.M., Ledru, P., 1992. Evolutions tectono-métamorphiques des nappes de l'Artense (Massif Central Français): nouveaux marqueurs de la collision dans la chaîne varisque. Bull. Soc. Géol. Fr. 163, 641–649.

Merlet, C., 1994. An accurate computer correction program for quantitative electron probe microanalysis. Mikrochim. Acta 114–115, 363–376.

Mollier, B., Bouchez, J.L., 1982. Structuration magmatique du complexe granitique de Brâme-St Sylvestre-St Goussaud (Limousin, Massif Central Français). C.R. Acad. Sci. Paris 294, 1329–1334.

Monié, P., Respaut, J.P., Brichau, S., Bouchot, V., Faure, M., Roig, J.Y., 2000. $^{40}Ar/^{39}Ar$ and U–Pb geochronology applied to Au–W–Sb metallogenesis in the Cévennes and Châtaigneraie districts (Southern Massif Central, France). In: Bouchot, V., Moritz, R. (Eds.), GEODE-GEOFRANCE 3D Workshop on Orogenic Gold Deposit in Europe with Emphasis on the Variscides., Orléans, pp. 77–79.

Montel, J.M., Marignac, C., Barbey, P., Pichavant, M., 1992. Thermobarometry and granite genesis: the Hercynian low-P, high T Velay anatectic dome (French Massif Central). J. Metamorph. Geol. 10, 1–15.

Mougeot, R., Respaut, J.P., Ledru, P., Marignac, C., 1997. U–Pb chronology on accessory minerals of the Velay anatectic dome (French Massif Central). Eur. J. Mineral. 9, 141–156.

Mulch, A., Chamberlain, C.P., 2007. Stable Isotope Paleoaltimetry in Orogenic Belts — the silicate record in surface and crustal geological archives. Rev. Mineral. Geochem. 66, 89–118.

Mulch, A., Teyssier, C., Cosca, M.A., Chamberlain, C.P., 2007. Stable isotope paleoaltimetry of Eocene core complexes in the North American Cordillera. Tectonics 26, TC4001. doi:10.1029/2006TC001995.

Ortega, L.A., Ibarguchi, J.I.G., 1990. The genesis of Late Hercynian granitoids (North-western Spain). Inferences from REE studies. J. Geol. 98, 189–212.

Paquette, J.L., Pin, C., 2001. A new miniaturized extraction chromatography method for precise U–Pb zircon geochronology. Chem. Geol. 176, 313–321.

Parrish, R.R., 1990. U–Pb dating of monazite and its application to geological problems. Can. J. Earth Sci. 27, 1431–1450.

Pelletier, A., Gapais, D., Ménot, R.P., Peucat, J.J., 2002. Tectonique transpressive en Terre Adélie au Paléoprotérozoïque (Est Antarctique). C.R. Acad. Sci. Paris 334, 505–511.

Petitpierre, E., Duthou, J.L., 1980. Age westphalien par la méthode Rb/Sr du leucogranite de Crevant, Plateau d'Aigurande (Massif Central Francais). C.R. Acad. Sci. Paris 163–166.

Pin, C., 1991. Sr–Nd isotopic study of igneous and metasedimentary enclaves in some hercynian granitoids from the Massif Central, France. In: Didier, J., Barbarin, B. (Eds.), Enclaves and granite petrology (Developments in Petrology), 13. Elsevier, pp. 333–343.

Pin, C., Vielzeuf, D., 1983. Granulites and related rocks in Variscan median Europe: a dualistic interpretation. Tectonophysics 93, 47–74.

Pupin, J.P., 1976. Signification des caractères morphologiques du zircon commun des roches en pétrologie. Bases de la méthode typologique. Applications, thèse d'Etat, Univ. Nice, 394 p.

Quenardel, J.M., Cohen-Julien, M., Freytet, P., Lemaire, D., Lerouge, G., Peulvast, J.P., Constans, J., Vautrelle, C., 1991. Notice de la carte géologique d'Aigurande à 1/50000. Editions BRGM, Orléans, 108 p.

Rey, P., Coltice, N., 2008. Neoarchean lithospheric strengthening and the coupling of Earth's geochemical reservoirs. Geology 36, 635–638.

Rey, P., Burg, J.P., Casey, M., 1997. The Scandinavian Caledonides and their relationship to the Variscan belt. In: Burg, J.P., Ford, M. (Eds.), Orogeny Through Time. Geol. Soc. Spec. Publ., 121, pp. 179–200.

Roger, F., Respaut, J.P., Brunel, M., Matte, P., Paquette, J.L., 2004. Première datation U–Pb des orthogneiss œillés de la zone axiale de la Montagne Noire (Sud du Massif Central): nouveaux témoins du magmatisme ordovicien dans la chaîne varisque. C.R. Acad. Sci. Paris 336, 19–28.

Rolin, P., Duthou, J.L., Quenardel, J.M., 1982. Datation Rb/Sr des leucogranites de Crozant et d'Orsennes: conséquences sur l'âge de la dernière phase de tectonique tangentielle du Plateau d'Aigurande (NW du Massif Central Français). C.R. Acad. Sci. Paris 294, 799–802.

Santallier, D., Briand, B., Ménot, R.P., Piboule, M., 1988. Les complexes leptyno-amphiboliques (C. L. A.): revue critique et suggestions pour un meilleur emploi de ce terme. C.R. Acad. Sci. Paris 8, 3–12.

Santallier, D., Lardeaux, J.M., Marchand, J., Marignac, C., 1994. Metamorphism. In: Keppie, J.D. (Ed.), Pre-Mesozoic Geology in France and Related Areas. Part III, The Massif Central. Springer Verlag, Berlin-Heidelberg, pp. 276–288.

Scaillet, S., Cuney, M., Le Carlier de Veslud, C., Cheilletz, A., Royer, J.J., 1996. Cooling pattern and mineralization history of the Saint Sylvestre and western Marche leucogranite pluton, French Massif Central: II. Thermal modelling and implications for the mechanisms of U-mineralization. Geochim. Cosmochim. Acta 60, 4673–4688.

Stacey, J.S., Kramers, J.D., 1975. Approximation of terrestrial lead isotope evolution by a two stage model. Earth Planet. Sci. Lett. 26, 207–221.

Steiger, R.H., Jäger, E., 1977. Subcommission on geochronology: convention on the use of decay constants in geo- and cosmochronology. Earth Planet. Sci. Lett. 36, 359–362.

Supply, J.P., 1985. Géochronologie U–Pb des granites du Morvan et de leurs minéralisations uranifères associées. Thèse 3ème cycle, Univ. Montpellier, 146 p.

Tapponnier, P., Lacassin, R., Leloup, P.H., Schärer, U., Dalai, Zhong, Xiaohan, Liu, Shaocheng, Ji, Lianshang, Zhang, Jiayou, Zhong, 1990. The Ailao Shan/Red River metamorphic belt: Tertiary left-lateral shear between Indochina and South China. Nature 343, 431–437.

Teyssier, C., Whitney, D.L., 2002. Gneiss domes and orogeny. Geology 30, 1139–1142.

Teyssier, C., Whitney, D.L., Rey, P., 2008. Dynamic coupling and coeval contraction/extension in and around orogenic plateaux. Eos Trans. AGU 89 (53) Fall Meet. Suppl., Abst. T23C-2040.

Thompson, P.H., Bard, J.P., 1982. Isograds and mineral assemblages in the Eastern axial zone, Montagne Noire (France). Implications for temperature gradients and P/T history. Can. J. Earth Sci. 19, 129–143.

Umhoefer, P.J., Whitney, D.L., Teyssier, C., Fayon, A.K., Casale, G., Heizler, M.T., 2007. Yo-yo tectonics in a wrench zone, central Anatolia. In: Till, A.B., Roeske, S., Sample, J.C., Foster, D. (Eds.), Exhumation and Continental Strike–Slip Fault Systems. Geol. Soc. Am. Spec. Pap., vol. 434, pp. 35–58.

Valle Aguado, V., Azevedo, M.R., Schaltegger, U., Martínez Catalán, J.R., Nolan, J., 2005. U–Pb zircon and monazite geochronology of Variscan magmatism related to syn-convergence extension in Central Northern Portugal. Lithos 82, 169–184.

Van Den Driessche, J., Brun, J.P., 1989. Un modèle de l'extension paléozoïque supérieur dans le Sud du Massif Central. C.R. Acad. Sci. Paris 309, 1607–1613.

Van Den Driessche, J., Brun, J.P., 1991. Tectonic evolution of the Montagne Noire (French Massif Central): a model of extensional gneiss dome. Geodin. Acta 5, 85–99.

Vanderhaeghe, O., Teyssier, C., 2001. Partial melting and flow of orogens. Tectonophysics 342, 451–472.

Vanderhaeghe, O., Burg, J.P., Teyssier, C., 1999. Exhumation of migmatites in two collapsed orogens. In: Ring, U., Brandon, M.T., Lister, G.S., Willet, S.D. (Eds.), Exhumation Processes: Normal Faulting, Ductile Flow and Erosion, Geol. Soc., London, Spec. Publ., vol. 154, pp. 181–204.

Vidal, P., 1976. L'évolution polyorogénique du Massif Armoricain: apport de la géochronologie et de la géochimie isotopique du Strontium. Thèse Sci. Nat., Univ. Rennes, 142 pp.

White, R.W., Powell, R., Halpin, J.A., 2004. Spatially-focused melt formation in aluminous metapelites from Broken hill, Australia. J. Metamorph. Geol. 22, 825–845.

White, R.W., Powell, R., Holland, T.J.B., 2007. Progress relating to calculation of partial melting equilibria for metapelites. J. Metamorph. Geol. 25, 511–527.

Whitney, D.L., Teyssier, C., Fayon, A.K., Hamilton, M.A., Heizler, M., 2003. Tectonic controls on metamorphism, partial melting, and intrusion: timing of regional metamorphism and magmatism of the Nigde Massif, Turkey. Tectonophysics 376, 37–60.

Whitney, D.L., Teyssier, C., Heizler, M.T., 2007. Gneiss domes, metamorphic core complexes, and wrench zones: thermal and structural evolution of the Nigde Massif, central Anatolia. Tectonics 26, TC5002. doi:10.1029/2006TC002040.

Williamson, B.J., Shaw, A., Downes, H., Thirlwall, M.F., 1996. Geochemical constraints on the genesis of Hercynian two-mica leucogranites from the Massif Central, France. Chem. Geol. 127, 25–42.